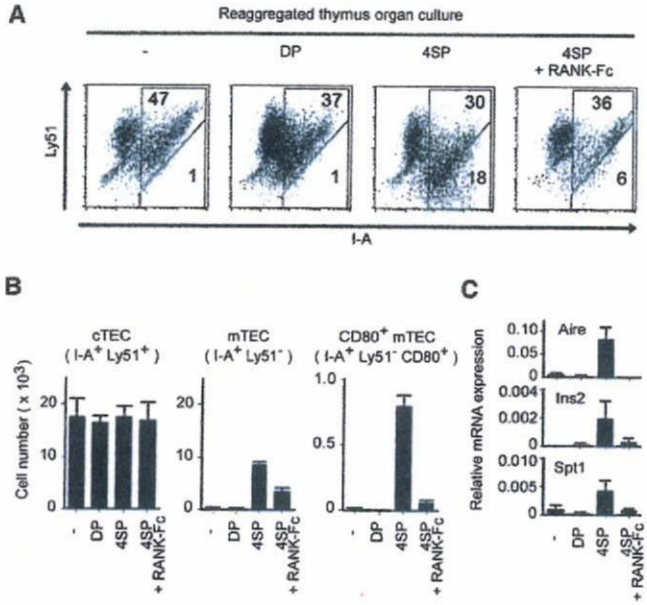

Figure 7. RANKL Produced by SP Thymocytes Promotes mTEC Cellularity in Reaggregated Thymus Organ Culture

dGuo-treated fetal thymic stromal cells (2.5×10^5) were reaggregated with equal numbers of either DP thymocytes from *Tcra*$^{-/-}$ mice or CD4SP thymocytes from B6 mice and organ cultured for 5 days. Where indicated, organ cultures included 5 μg/ml of RANK-Fc fusion protein. Cells were analyzed by flow cytometry (A and B) or quantitative RT-PCR (C).

(A) Representative two-color flow cytometry profiles for I-A and Ly51 of CD45$^-$ nonleukocytes. Numbers indicate frequency of cells within indicated areas.

(B) Numbers of indicated TEC populations per reaggregated thymus organ culture. Averages and standard errors (n = 4–5) are shown.

(C) Quantitative RT-PCR analysis of indicated genes. mRNA expression was normalized to GAPDH mRNA, and those in CD45$^-$I-A$^+$UEA1$^+$ mTECs isolated from adult thymus were arbitrarily set to 1. Averages and standard errors of 4–5 independent measurements are shown.

formation of thymic medulla containing Aire-expressing mTECs. In the absence of positive selection, not only is T lymphocyte development arrested at the DP thymocyte stage, but medulla formation is impaired as well. Through gene-expression analysis of positively selected thymocytes and thymic epithelial cells, we found that RANKL is produced by positively selected thymocytes and that RANKL receptors, RANK and OPG, are expressed by mTECs rather than by cTECs. Mice deficient for RANKL showed a reduction in the number of mTECs, whereas mice deficient for OPG showed a large number of mTECs and a large thymic medulla. Although RANKL expression in the thymus is also detectable in TCR$\gamma\delta^+$ cells and CD4$^+$CD3$^-$ LTi cells, these cells appear dispensable for mTEC generation and medulla formation. The blockade of RANKL perturbs mTEC cellularity in normal mice, whereas forced expression of RANKL restores mTEC cellularity and medulla formation in mice lacking positive selection. These results indicate that RANKL produced by positively selected thymocytes plays a major role in the increase in the number of mTECs and the formation of thymic medulla that contains Aire-expressing mTECs.

Several studies have shown that positively selected thymocytes produce signals crucial for thymic medulla formation (Shores et al., 1991; Surh et al., 1992; Naspetti et al., 1997; Nasreen et al., 2003). However, it was unclear whether positive selection regulates the genesis or increase in number of functionally competent mTECs. The present results show that the lack of positive selection reduces the number of mTECs, whereas small numbers of mTECs detectable in mice lacking positive selection contain Aire-expressing cells and CCL21-expressing cells. Aire and CCL21 are two major molecules that are vital to the execution of thymic medulla function to induce central tolerance, by displaying a diverse set of tissue-restricted genes (Derbinski et al., 2001) and by attracting CCR7-expressing positively selected cortical thymocytes toward the medulla (Ueno et al., 2004), respectively. Indeed, our results show that mTECs generated without positive selection exhibit a gene-expression profile that is characteristic of promiscuous gene expression. These results support the notion that positive selection affects the formation of thymic medulla by promoting the increase in the number of functionally competent mTECs rather than by inducing the functional maturation of mTECs. These results also suggest that thymic medulla formation consists of two sequential processes: initial maturation of mTECs independent of positive selection and subsequent increase in the number of mTECs, which is dependent on positively selected thymocytes. Our results showing that RANKL expression in bone-marrow-derived cells causes elevated proliferation of mTECs without positive selection suggest that RANKL contributes to enhancing mTEC proliferation.

Through microarray data search for genes that are highly expressed upon positive selection, we found that the expression of eight TNFSF genes encoding LTα, TNFα, LTβ, OX40L, CD40L, FasL, CD30L, and RANKL was elevated during the differentiation of DP thymocytes into SP thymocytes. Subsequent survey of genes that are more strongly expressed in mTECs than in cTECs showed that five TNFSF ligand-receptor combinations, namely, between OX40L and OX40, between CD40L and CD40, between FasL and Fas, between CD30L and CD30, and among RANKL, RANK, and OPG, represent combinations in which the ligands are more strongly expressed in SP thymocytes than in DP thymocytes and the receptors are more strongly expressed in mTECs than in cTECs. Analysis of mTEC number and medulla formation in mice deficient for one of these molecules showed that the interaction among RANKL, RANK, and OPG critically regulates the increase in the number of mTECs that leads to medulla formation. Even though the present results obtained via mice deficient for OX40L, CD40, Fas, FasL, or CD30L did not reveal the role of these molecules in regulating mTEC cellularity or medulla formation, our study does not exclude the possibility that these molecules may also be involved in regulating medulla formation. Previous studies of the roles of LTβR (Boehm et al., 2003; Chin et al., 2003; Venanzi et al., 2007) and CD40L (Dunn et al., 1997; Clegg et al., 1997) in medulla development suggest the role of additional TNFSF ligands other than RANKL in generating normal thymic medulla. Indeed, our results indicate that the number of mTECs in RANKL-deficient mice is larger than that in TCRα-deficient or ZAP70-deficient mice, suggesting that the increase in mTEC cellularity caused by positively selected thymocytes may be additionally regulated by signals other than RANKL.

Accordingly, Akiyama et al. (2008) in this issue of *Immunity* found the cooperative roles of CD40L and RANKL in postnatal

medulla formation, by showing that mTEC development is more severely affected in mice doubly deficient for RANKL and CD40 than in RANKL-deficient mice. In CD40-deficient mice, the absolute number of mTECs is not reduced, yet the frequency of class II MHC^{lo} subsets of mTECs is reduced (Akiyama et al., 2008). Thus, the defect in mTECs is much milder in CD40-deficient mice than in RANKL-deficient mice. The reduced frequency of class II MHC^{lo} subsets of mTECs was also reported in CD40L-deficient mice (Gray et al., 2006). We think that RANKL and CD40 at least partially compensate each other but unequally contribute to mTEC development, in which RANKL and CD40L play major and minor roles, respectively.

The intrathymic expression profiles of CD40L and CD40 are somewhat similar to those of RANKL and RANK, respectively; CD40L is highly detectable in positively selected thymocytes and CD4$^+$CD3$^-$ cells, whereas CD40 is more strongly detectable in mTECs than in cTECs (Figure S6). However, unlike RANKL, CD40L is not prominently detectable in TCR$\gamma\delta^+$ cells, and unlike RANK, CD40 is also detectable in CD11c$^+$ DC (Figure S6), indicating that the expression profiles of CD40L and CD40 in the thymus are not exactly identical to those of RANKL and RANK. The unequal roles of CD40L and RANKL in the thymus are also evident from our results that, unlike the retroviral expression of RANKL, that of CD40L dramatically reduces thymocyte cellularity and does not elevate mTEC cellularity in bone marrow chimeras (Figure S7). The reduction in thymocyte cellularity was also reported in proximal *Lck* promoter driven CD40L-transgenic thymocytes (Dunn et al., 1997; Clegg et al., 1997). Thus, it appears that CD40L-overexpressing immature thymocytes are inefficient in survival and/or proliferation, further suggesting that RANKL and CD40L play unequal functions in the thymus.

Our results show that the number of mTECs is reduced in the thymus of RANKL-deficient mice, whereas the number of mTECs is increased in the thymus of OPG-deficient mice. The expression of Aire and CCL21 in mTECs is detectable either in RANKL-deficient mice or in OPG-deficient mice. These results suggest that similar to positively selected thymocytes, RANKL regulates the cellularity, rather than the genesis, of functional mTECs. We also found that in vivo blockade of RANKL by a RANK-Fc fusion protein reduces the number of mTECs in normal mice even in the presence of positive selection, whereas forced expression of RANKL in mice deficient for positive selection restores the number of mTEC and medulla formation in vivo. Our results further show that RANKL is expressed in positively selected thymocytes and in TCR-stimulated DP thymocytes. On the other hand, RANKL is produced as a transmembrane cell-surface protein and can be released as a secreted protein from cell surface (Nakashima et al., 2000). Thus, it is conceivable that positive selection of thymocytes in the thymic cortex elevates the expression of RANKL, which acts to increase the number of mTECs even if mTECs may be remotely localized from positively selected thymocytes. Positive selection also induces CCR7 expression by cortical thymocytes, thereby causing the relocation of positively selected thymocytes to the medulla where mTECs produce CCR7 ligands (Ueno et al., 2004; Kurobe et al., 2006). Thus, positive selection signals increase the expression of RANKL and CCR7, thereby directly regulating both the formation of medullary microenvironment where mTECs express RANKL receptors and the migration of positively selected thymocytes toward the medulla where mTECs express CCR7 ligands.

In agreement with our results, Rossi et al. (2007) recently reported that the number of Aire-expressing mTECs was severely reduced in RANK-deficient mice. They also reported that RANKL is produced by CD4$^+$CD3$^-$ LTi cells in the thymus and that the appearance of CD4$^+$CD3$^-$ LTi cells coincides with the appearance of Aire-expressing mTECs during embryogenesis, suggesting that RANKL-expressing CD4$^+$CD3$^-$ LTi cells induce the generation of Aire-expressing mTECs during embryogenesis (Rossi et al., 2007). Our results indeed show that among adult thymocyte subpopulations, CD4$^+$CD3$^-$ LTi cells and TCR$\gamma\delta^+$ cells, in addition to positively selected thymocytes, produce RANKL. However, our results also show that unlike mice lacking positive selection, Id2-deficient mice lacking Id2-dependent LTi cells or TCRδ-deficient mice lacking TCR$\gamma\delta^+$ cells exhibit no impairment in the number of Aire-expressing mTECs and in the formation of thymic medulla in adult mice. Thus, Id2-dependent CD4$^+$CD3$^-$ LTi cells or TCR$\gamma\delta^+$ cells are dispensable for the formation of thymic medulla containing Aire-expressing mTECs in adult thymus. It is possible that LTi cells and/or TCR$\gamma\delta^+$ cells may primarily participate in the generation of mTEC during embryogenesis rather than during postnatal period, and/or LTi cells involved in thymic medulla development may be generated independent of Id2. It is also possible that any cell type expressing RANKL may be sufficient to influence the cellularity of mTECs and that the contribution of positively selected thymocytes may be best highlighted in postnatal thymus, perhaps because SP thymocytes are present in much larger number than other RANKL-expressing cells, such as LTi and TCR$\gamma\delta$ cells.

Our results reveal a role for OPG in thymic medulla formation. OPG is an osteoclastogenesis inhibitory protein that lacks a transmembrane domain and is a secreted decoy receptor for RANKL (Mizuno et al., 1998; Theill et al., 2002). We found that similar to RANK, OPG is strongly expressed in mTECs rather than in cTECs or other cell types within the thymus. We also showed that the deficiency in OPG causes an increase in mTEC number and enlargement of the thymic medulla. These results suggest that OPG-mediated fine-tuning of RANKL availability at mTEC surface crucially regulates RANK-mediated signals in mTECs, perhaps through TRAF6 and NF-κB, to increase the number of mTECs and form thymic medulla.

In conclusion, this study shows that RANKL produced by positively selected thymocytes plays a pivotal role in increasing the number of mTECs and forming thymic medulla that contains Aire-expressing mTECs. The results demonstrate that RANKL represents a major mediator of thymic crosstalk for the formation of medullary microenvironment by positively selected thymocytes. By increasing the number of Aire-expressing mTECs through RANKL, positively selected thymocytes may pave their own way for subsequent developmental regulation in the medulla to establish central tolerance. Indeed, lymphocytes generated without RANKL fail to establish self-tolerance because these cells manifest infiltration and antibody deposition in the liver (Akiyama et al., 2008). Lymphocytes generated without both RANKL and CD40 cause more severe autoimmune phenotypes than those generated without RANKL alone, whereas lymphocytes from CD40-deficient mice exhibit no detectable autoimmunity. Therefore, the severity of autoimmunity among

these mice appears to be well correlated with the defects in mTEC development. Further studies geared toward revealing the molecular mechanisms of TEC development and thymic microenvironment formation are expected to aid in improving our understanding of and controlling diverse and self-tolerant repertoire formation of T lymphocytes.

EXPERIMENTAL PROCEDURES

Mice

C57BL/6 (B6), BALB/c, ICR, B6-*Fasl*$^{gld/gld}$, and B6-*Fas*$^{lpr/lpr}$ mice were purchased from SLC Japan. *Tnfrsf11b*$^{-/-}$ mice (Mizuno et al., 1998) were purchased from CLEA Japan. *Tcra*$^{-/-}$ (Mombaerts et al., 1992), *Zap70*$^{-/-}$ (Negishi et al., 1995), *Rag2*$^{-/-}$ (Shinkai et al., 1993), *Relb*$^{-/-}$ (Burkly et al., 1995), *Tnfsf4*$^{-/-}$ (Murata et al., 2000), *Cd40*$^{-/-}$ (Kawabe et al., 1994), *Tnfsf8*$^{-/-}$ (Blazar et al., 2004), *Tnfsf11*$^{-/-}$ (Kong et al., 1999), *H2-Ab1*$^{-/-}$ (Cosgrove et al., 1991), *B2m*$^{-/-}$ (Koller et al., 1990), *Tcrd*$^{-/-}$ (Itohara et al., 1993), *Id2*$^{-/-}$ (Yokota et al., 1999), and *Rorc*$^{-/-}$ (Sun et al., 2000) mice were previously described. Experiments with mice were performed with consent from the Animal Experimentation Committee of the University of Tokushima.

Retrovirus Infection

PCR-cloned cDNA fragments encoding an open-reading frame of mouse RANKL, OX40L, CD30L, CD40L, or FasL were cloned in the retrovirus vector pMSCV-IRES-EGFP (Nitta et al., 2006). To construct retrovirus vector expressing RANK-Fc, a cDNA fragment encoding the extracellular region of RANK (aa 1–212) was ligated with human IgG1 Fc cDNA (Zettlmeissl et al., 1990) and inserted into pMSCV-IRES-EGFP. Retroviral production and infection were performed as previously described (Ueno et al., 2005). To generate irradiation bone marrow chimeras, bone marrow cells were harvested from donor mice 4 days after intravenous administration of 5-fluorouracil (150 mg/kg). Sca1$^+$ cells were sorted and precultured in growth medium (Iscove's modified Dulbecco's medium containing 20% FCS, L-glutamine, sodium pyruvate, nonessential amino acids, penicillin, streptomycin, 50 ng/ml SCF, 50 ng/ml IL-6, and 10 ng/ml IL-3). 48 hr later, the culture medium was replaced with retroviral supernatants containing 10 μg/ml polybrene, and culture plates were centrifuged at 1000 × g for 90 min at 30°C. Cells were replenished with the growth medium, cultured overnight, and additionally infected at 24 and 48 hr. Cells were intravenously injected into lethally irradiated (9.0 Gy) recipient mice.

Thymus Section Analysis

Frozen thymuses embedded in OCT compound (Sakura Finetek) were sliced into 5 μm-thick sections and stained with hematoxylin and eosin. For multicolor confocal analysis, frozen sections were fixed with acetone and stained with the following antibodies: mTEC-specific ER-TR5 followed by Alexa Fluor 633-conjugated anti-rat IgG antibody (Molecular Probes); anti-Aire antibody (Santa Cruz) followed by FITC- or Alexa Fluor 568-conjugated anti-rabbit IgG antibody (Molecular Probes); biotinylated anti-CCL21 antibody (R&D Systems) or *Ulex europaeus* agglutinin 1 (UEA1) (Vector Laboratories) followed by Alexa Fluor 488- or Alexa Fluor 546-conjugated streptavidin (Molecular Probes). Images were analyzed with TSC SP2 confocal laser-scanning microscope and Leica Confocal software (version 2.6, Leica).

Flow Cytometry Analysis and Sorting of Thymic Stromal Cells

Multicolor flow cytometry analysis and cell sorting were performed with FACSCalibur and FACS-Vantage (BD Biosciences) as described (Ueno et al., 2005). Thymic stromal cells were prepared by digesting thymic fragments with collagenase, dispase, and DNase I (Roche), as described (Gray et al., 2002). For TEC analysis, cells were stained with allophycocyanin-conjugated antibody specific for CD45, FITC-conjugated antibody specific for I-A (or antibody specific for I-E where indicated), and biotinylated UEA1 or biotinylated antibody specific for Ly51 followed by phycoerythrin-conjugated streptavidin. For TEC sorting, CD45$^-$ cells were enriched by depleting CD45$^+$ cells with a magnetic cell sorter (Miltenyi Biotec) prior to FACS cell sorting. Monoclonal antibody specific for RANKL (BioLegend #510003) was used to detect RANKL expression on cell surface. Ki67 expression, bromodeoxyuridine (BrdU) incorporation, and TdT-mediated dUTP nick end labeling (TUNEL) were measured according to the manufacturers' instructions.

Quantitative mRNA Analysis

Total cellular RNA was reverse-transcribed with oligo-dT primer and Superscript III reverse transcriptase (Invitrogen). Real-time RT-PCR was performed with SYBR Premix Ex Taq (TaKaRa) and Light Cycler DX400 (Roche). Amplified signals were confirmed to be single bands over gel electrophoresis, and normalized to GAPDH. Primer sequences are listed in Table S2.

Reaggregated Thymus Organ Culture

Thymic stromal cells isolated from E15.5 fetal thymus lobes that were cultured for 6 days in the presence of 2-deoxyguanosine (dGuo) were reaggregated with equal numbers of either DP thymocytes isolated from adult TCRα-deficient mice or CD4SP thymocytes isolated from adult B6 mice, and organ cultured for 5 days as previously described (Ueno et al., 2005). RANK-Fc fusion protein was produced by transfected 293T cells and purified with protein A-Sepharose (Amersham-Pharmacia).

SUPPLEMENTAL DATA

Supplemental Data include seven figures and two tables and can be found with this article online at http://www.immunity.com/cgi/content/full/29/3/438/DC1/.

ACKNOWLEDGMENTS

We thank H. Kikutani, T. Yasui, K. Sugamura, N. Ishii, D. Littman, S. Fagarasan, E. Podack, I. Negishi, S. Itohara, and M. Nanno for generously providing us the mice used in this study. We thank H. Nakase, T. Ueno, and Q. Cui for critically reading the manuscript. Technical support by S. Nitta is acknowledged. This study was supported by MEXT Grant-in-Aid for Scientific Research on Priority Areas "Immunological Self" and the Mitsubishi Foundation. Y.H. is a visiting graduate student from Nagoya City University Graduate School of Medical Sciences. T.N. is a JSPS Research Fellow.

Received: December 7, 2007
Revised: April 8, 2008
Accepted: June 20, 2008
Published online: September 18, 2008

REFERENCES

Akiyama, T., Maeda, S., Yamane, S., Ogino, K., Kasai, M., Kajiura, F., Matsumoto, M., and Inoue, J. (2005). Dependence of self-tolerance on TRAF6-directed development of thymic stroma. Science *308*, 248–251.

Akiyama, T., Shimo, Y., Yanai, H., Qin, J., Ohshima, D., Maruyama, Y., Asaumi, Y., Kitazawa, J., Takayanagi, H., Penninger, J.M., et al. (2008). The tumor necrosis factor family receptors RANK and CD40 cooperatively establish the thymic medullary microenvironment and self-tolerance. Immunity *29*, this issue, 423–437.

Anderson, M.S., Venanzi, E.S., Klein, L., Chen, Z., Berzins, S.P., Turley, S.J., von Boehmer, H., Bronson, R., Dierich, A., Benoist, C., and Mathis, D. (2002). Projection of an immunological self shadow within the thymus by the aire protein. Science *298*, 1395–1401.

Bendelac, A., Matzinger, P., Seder, R.A., Paul, W.E., and Schwartz, R.H. (1992). Activation events during thymic selection. J. Exp. Med. *175*, 731–742.

Blazar, B.R., Levy, R.B., Mak, T.W., Panoskaltsis-Mortari, A., Muta, H., Jones, M., Roskos, M., Serody, J.S., Yagita, H., Podack, E.R., and Taylor, P.A. (2004). CD30/CD30 ligand (CD153) interaction regulates CD4+ T cell-mediated graft-versus-host disease. J. Immunol. *173*, 2933–2941.

Bleul, C.C., Corbeaux, T., Reuter, A., Fisch, P., Monting, J.S., and Boehm, T. (2006). Formation of a functional thymus initiated by a postnatal epithelial progenitor cell. Nature *441*, 992–996.

Boehm, T., Scheu, S., Pfeffer, K., and Bleul, C.C. (2003). Thymic medullary epithelial cell differentiation, thymocyte emigration, and the control of autoimmunity require lympho-epithelial cross talk via LTβR. J. Exp. Med. *198*, 757–769.

Bonasio, R., Scimone, M.L., Schaerli, P., Grabie, N., Lichtman, A.H., and von Andrian, U.H. (2006). Clonal deletion of thymocytes by circulating dendritic cells homing to the thymus. Nat. Immunol. *7*, 1092–1100.

Burkly, L., Hession, C., Ogata, L., Reilly, C., Marconi, L.A., Olson, D., Tizard, R., Cate, R., and Lo, D. (1995). Expression of relB is required for the development of thymic medulla and dendritic cells. Nature *373*, 531–536.

Chin, R.K., Lo, J.C., Kim, O., Blink, S.E., Christiansen, P.A., Peterson, P., Wang, Y., Ware, C., and Fu, Y.X. (2003). Lymphotoxin pathway directs thymic Aire expression. Nat. Immunol. *4*, 1121–1127.

Clegg, C.H., Rulffes, J.T., Haugen, H.S., Hoggatt, I.H., Aruffo, A., Durham, S.K., Farr, A.G., and Hollenbaugh, D. (1997). Thymus dysfunction and chronic inflammatory disease in gp39 transgenic mice. Int. Immunol. *9*, 1111–1122.

Cosgrove, D., Gray, D., Dierich, A., Kaufman, J., Lemeur, M., Benoist, C., and Mathis, D. (1991). Mice lacking MHC class II molecules. Cell *66*, 1051–1066.

Daniels, M.A., Teixeiro, E., Gill, J., Hausmann, B., Roubaty, D., Holmberg, K., Werlen, G., Hollander, G.A., Gascoigne, N.R., and Palmer, E. (2006). Thymic selection threshold defined by compartmentalization of Ras/MAPK signalling. Nature *444*, 724–729.

Derbinski, J., Schulte, A., Kyewski, B., and Klein, L. (2001). Promiscuous gene expression in medullary thymic epithelial cells mirrors the peripheral self. Nat. Immunol. *2*, 1032–1039.

Dunn, R.J., Luedecker, C.J., Haugen, H.S., Clegg, C.H., and Farr, A.G. (1997). Thymic overexpression of CD40 ligand disrupts normal thymic epithelial organization. J. Histochem. Cytochem. *45*, 129–141.

Eberl, G., Marmon, S., Sunshine, M.J., Rennert, P.D., Choi, Y., and Littman, D.R. (2004). An essential function for the nuclear receptor RORγt in the generation of fetal lymphoid tissue inducer cells. Nat. Immunol. *5*, 64–73.

Finkel, T.H., Cambier, J.C., Kubo, R.T., Born, W.K., Marrack, P., and Kappler, J.W. (1989). The thymus has two functionally distinct populations of immature $\alpha\beta^+$ T cells: one population is deleted by ligation of αβ TCR. Cell *58*, 1047–1054.

Gallegos, A.M., and Bevan, M.J. (2004). Central tolerance to tissue-specific antigens mediated by direct and indirect antigen presentation. J. Exp. Med. *200*, 1039–1049.

Gray, D.H., Chidgey, A.P., and Boyd, R.L. (2002). Analysis of thymic stromal cell populations using flow cytometry. J. Immunol. Methods *260*, 15–28.

Gray, D.H., Seach, N., Ueno, T., Milton, M.K., Liston, A., Lew, A.M., Goodnow, C.C., and Boyd, R.L. (2006). Developmental kinetics, turnover, and stimulatory capacity of thymic epithelial cells. Blood *108*, 3777–3785.

Hamazaki, Y., Fujita, H., Kobayashi, T., Choi, Y., Scott, H.S., Matsumoto, M., and Minato, N. (2007). Medullary thymic epithelial cells expressing Aire represent a unique lineage derived from cells expressing claudin. Nat. Immunol. *8*, 304–311.

Honey, K., Nakagawa, T., Peters, C., and Rudensky, A. (2002). Cathepsin L regulates $CD4^+$ T cell selection independently of its effect on invariant chain: A role in the generation of positively selecting peptide ligands. J. Exp. Med. *195*, 1349–1358.

Hsu, H., Lacey, D.L., Dunstan, C.R., Solovyev, I., Colombero, A., Timms, E., Tan, H.L., Elliott, G., Kelley, M.J., Sarosi, I., et al. (1999). Tumor necrosis factor receptor family member RANK mediates osteoclast differentiation and activation induced by osteoprotegerin ligand. Proc. Natl. Acad. Sci. USA *96*, 3540–3545.

Itohara, S., Mombaerts, P., Lafaille, J., Iacomini, J., Nelson, A., Clarke, A.R., Hooper, M.L., Farr, A., and Tonegawa, S. (1993). T cell receptor δ gene mutant mice: Independent generation of αβ T cells and programmed rearrangements of γδ TCR genes. Cell *72*, 337–348.

Kawabe, T., Naka, T., Yoshida, K., Tanaka, T., Fujiwara, H., Suematsu, S., Yoshida, N., Kishimoto, T., and Kikutani, H. (1994). The immune responses in CD40-deficient mice: Impaired immunoglobulin class switching and germinal center formation. Immunity *1*, 167–178.

Kisielow, P., Teh, H.S., Bluthmann, H., and von Boehmer, H. (1988). Positive selection of antigen-specific T cells in thymus by restricting MHC molecules. Nature *335*, 730–733.

Koller, B.H., Marrack, P., Kappler, J.W., and Smithies, O. (1990). Normal development of mice deficient in β2M, MHC class I proteins, and $CD8^+$ T cells. Science *248*, 1227–1230.

Kong, Y.Y., Yoshida, H., Sarosi, I., Tan, H.L., Timms, E., Capparelli, C., Morony, S., Oliveira-dos-Santos, A.J., Van, G., Itie, A., et al. (1999). OPGL is a key regulator of osteoclastogenesis, lymphocyte development and lymph-node organogenesis. Nature *397*, 315–323.

Kurobe, H., Liu, C., Ueno, T., Saito, F., Ohigashi, I., Seach, N., Arakaki, R., Hayashi, Y., Kitagawa, T., Lipp, M., et al. (2006). CCR7-dependent cortex-to-medulla migration of positively selected thymocytes is essential for establishing central tolerance. Immunity *24*, 165–177.

Kwan, J., and Killeen, N. (2004). CCR7 directs the migration of thymocytes into the thymic medulla. J. Immunol. *172*, 3999–4007.

Mizuno, A., Amizuka, N., Irie, K., Murakami, A., Fujise, N., Kanno, T., Sato, Y., Nakagawa, N., Yasuda, H., Mochizuki, S., et al. (1998). Severe osteoporosis in mice lacking osteoclastogenesis inhibitory factor/osteoprotegerin. Biochem. Biophys. Res. Commun. *247*, 610–615.

Mombaerts, P., Clarke, A.R., Rudnicki, M.A., Iacomini, J., Itohara, S., Lafaille, J.J., Wang, L., Ichikawa, Y., Jaenisch, R., Hooper, M.L., and Tonegawa, S. (1992). Mutations in T-cell antigen receptor genes α and β block thymocyte development at different stages. Nature *360*, 225–231.

Murata, K., Ishii, N., Takano, H., Miura, S., Ndhlovu, L.C., Nose, M., Noda, T., and Sugamura, K. (2000). Impairment of antigen-presenting cell function in mice lacking expression of OX40 ligand. J. Exp. Med. *191*, 365–374.

Murata, S., Sasaki, K., Kishimoto, T., Niwa, S., Hayashi, H., Takahama, Y., and Tanaka, K. (2007). Regulation of $CD8^+$ T cell development by thymus-specific proteasomes. Science *316*, 1349–1353.

Nakashima, T., Kobayashi, Y., Yamasaki, S., Kawakami, A., Eguchi, K., Sasaki, H., and Sakai, H. (2000). Protein expression and functional difference of membrane-bound and soluble receptor activator of NF-κB ligand: Modulation of the expression by osteotropic factors and cytokines. Biochem. Biophys. Res. Commun. *275*, 768–775.

Naspetti, M., Aurrand-Lions, M., DeKoning, J., Malissen, M., Galland, F., Lo, D., and Naquet, P. (1997). Thymocytes and RelB-dependent medullary epithelial cells provide growth-promoting and organization signals, respectively, to thymic medullary stromal cells. Eur. J. Immunol. *27*, 1392–1397.

Nasreen, M., Ueno, T., Saito, F., and Takahama, Y. (2003). In vivo treatment of class II MHC-deficient mice with anti-TCR antibody restores the generation of circulating CD4 T cells and optimal architecture of thymic medulla. J. Immunol. *171*, 3394–3400.

Negishi, I., Motoyama, N., Nakayama, K., Nakayama, K., Senju, S., Hatakeyama, S., Zhang, Q., Chan, A.C., and Loh, D.Y. (1995). Essential role for ZAP-70 in both positive and negative selection of thymocytes. Nature *376*, 435–438.

Nitta, T., Nasreen, M., Seike, T., Goji, A., Ohigashi, I., Miyazaki, T., Ohta, T., Kanno, M., and Takahama, Y. (2006). IAN family critically regulates survival and development of T lymphocytes. PLoS Biol. *4*, e103.

Philpott, K.L., Viney, J.L., Kay, G., Rastan, S., Gardiner, E.M., Chae, S., Hayday, A.C., and Owen, M.J. (1992). Lymphoid development in mice congenitally lacking T cell receptor αβ-expressing cells. Science *256*, 1448–1452.

Rossi, S.W., Jenkinson, W.E., Anderson, G., and Jenkinson, E.J. (2006). Clonal analysis reveals a common progenitor for thymic cortical and medullary epithelium. Nature *441*, 988–991.

Rossi, S.W., Kim, M.Y., Leibbrandt, A., Parnell, S.M., Jenkinson, W.E., Glanville, S.H., McConnell, F.M., Scott, H.S., Penninger, J.M., Jenkinson, E.J., et al. (2007). RANK signals from $CD4^+3^-$ inducer cells regulate development of Aire-expressing epithelial cells in the thymic medulla. J. Exp. Med. *204*, 1267–1272.

Shinkai, Y., Koyasu, S., Nakayama, K., Murphy, K.M., Loh, D.Y., Reinherz, E.L., and Alt, F.W. (1993). Restoration of T cell development in RAG-2-deficient mice by functional TCR transgenes. Science *259*, 822–825.

Shores, E.W., Van Ewijk, W., and Singer, A. (1991). Disorganization and restoration of thymic medullary epithelial cells in T cell receptor-negative scid mice:

Evidence that receptor-bearing lymphocytes influence maturation of the thymic microenvironment. Eur. J. Immunol. *21*, 1657–1661.

Sun, Z., Unutmaz, D., Zou, Y.R., Sunshine, M.J., Pierani, A., Brenner-Morton, S., Mebius, R.E., and Littman, D.R. (2000). Requirement for RORγ in thymocyte survival and lymphoid organ development. Science *288*, 2369–2373.

Surh, C.D., Ernst, B., and Sprent, J. (1992). Growth of epithelial cells in the thymic medulla is under the control of mature T cells. J. Exp. Med. *176*, 611–616.

Takahama, Y., and Nakauchi, H. (1996). Phorbol ester and calcium ionophore can replace TCR signals that induce positive selection of CD4 T cells. J. Immunol. *157*, 1508–1513.

Theill, L.E., Boyle, W.J., and Penninger, J.M. (2002). RANK-L and RANK: T cells, bone loss, and mammalian evolution. Annu. Rev. Immunol. *20*, 795–823.

Ueno, T., Saito, F., Gray, D.H., Kuse, S., Hieshima, K., Nakano, H., Kakiuchi, T., Lipp, M., Boyd, R.L., and Takahama, Y. (2004). CCR7 signals are essential for cortex-medulla migration of developing thymocytes. J. Exp. Med. *200*, 493–505.

Ueno, T., Liu, C., Nitta, T., and Takahama, Y. (2005). Development of T-lymphocytes in mouse fetal thymus organ culture. Methods Mol. Biol. *290*, 117–133.

van Ewijk, W., Shores, E.W., and Singer, A. (1994). Crosstalk in the mouse thymus. Immunol. Today *15*, 214–217.

Venanzi, E.S., Gray, D.H., Benoist, C., and Mathis, D. (2007). Lymphotoxin pathway and Aire influences on thymic medullary epithelial cells are unconnected. J. Immunol. *179*, 5693–5700.

Yokota, Y., Mansouri, A., Mori, S., Sugawara, S., Adachi, S., Nishikawa, S., and Gruss, P. (1999). Development of peripheral lymphoid organs and natural killer cells depends on the helix-loop-helix inhibitor Id2. Nature *397*, 702–706.

Zettlmeissl, G., Gregersen, J.P., Duport, J.M., Mehdi, S., Reiner, G., and Seed, B. (1990). Expression and characterization of human CD4:immunoglobulin fusion proteins. DNA Cell Biol. *9*, 347–353.

Expression of the retinoblastoma protein RbAp48 in exocrine glands leads to Sjögren's syndrome–like autoimmune exocrinopathy

Naozumi Ishimaru,[1] Rieko Arakaki,[1] Satoko Yoshida,[1] Akiko Yamada,[1] Sumihare Noji,[2] and Yoshio Hayashi[1]

[1]Department of Oral Molecular Pathology, Institute of Health Biosciences, [2]Department of Life Systems, Institute of Technology and Science, The University of Tokushima Graduate School, Tokushima 770-8504, Japan

Although several autoimmune diseases are known to develop in postmenopausal women, the mechanisms by which estrogen deficiency influences autoimmunity remain unclear. Recently, we found that retinoblastoma-associated protein 48 (RbAp48) induces tissue-specific apoptosis in the exocrine glands depending on the level of estrogen deficiency. In this study, we report that transgenic (Tg) expression of RbAp48 resulted in the development of autoimmune exocrinopathy resembling Sjögren's syndrome. CD4+ T cell–mediated autoimmune lesions were aggravated with age, in association with autoantibody productions. Surprisingly, we obtained evidence that salivary and lacrimal epithelial cells can produce interferon-γ (IFN-γ) in addition to interleukin-18, which activates IFN regulatory factor-1 and class II transactivator. Indeed, autoimmune lesions in *Rag2*$^{-/-}$ mice were induced by the adoptive transfer of lymph node T cells from *RbAp48*-Tg mice. These results indicate a novel immunocompetent role of epithelial cells that can produce IFN-γ, resulting in loss of local tolerance before developing gender-based autoimmunity.

CORRESPONDENCE
Yoshio Hayashi:
hayashi@dent.tokushima-u.ac.jp

Abbreviations used: CIITA, class II transactivator; cLN, cervical LN; HSG, human salivary gland; IRF, IFN regulatory factor; MSG, mouse salivary gland; NOD, nonobese diabetic; RA, rheumatoid arthritis; RbAp48, retinoblastoma-associated protein 48; SLE, systemic lupus erythematosus; SS, Sjögren's syndrome; Tg, transgenic.

Autoimmune disease is controlled by environments that include gene variants or various cytokines (1, 2). It can increase susceptibility to autoimmunity by affecting the overall reactivity and quality of the cells of the immune system. There is an autoimmune disease specific for certain organs in the body, involving a response to an antigen expressed only in those organs. Antigen/organ specificity is affected by antigen presentation and recognition, antigen expression, and the state and response of the target organs (3, 4), which are maintained by a local immune system termed here "local tolerance."

Many mechanisms protect tissues from autoimmune damage. These include relative isolation from the immune system and inhibition of the function of invading lymphocytes. For example, the eye has barriers to T cell infiltration and produces immunosuppressive cytokines, such as TGF-β (5). Constitutive expression of Fas ligand within the privileged site might also prevent immune-mediated damage by eliminating Fas-expressing T cells (6). Although they have yet to be well demonstrated in spontaneous animal models or human disease, genetic effects at the level of tissue protection are therefore to be expected. Autoimmune organ damage can be mediated by CD4+ T cells, which play a crucial role in the development of autoimmunity (7–9). MHC class II alleles are probably involved in autoimmune disease because different alleles have different abilities to present peptides from target cells to autoreactive CD4+ T cells (10, 11). Certain class II alleles might predispose to autoimmunity by increasing positive selection or decreasing negative selection of autoreactive T cells in the thymus. They might also act by inhibiting selection in the thymus of the regulatory CD4+ T cells that are thought to prevent autoantigen-specific responses. Evidence for the local tolerance hypothesis is provided by the observation that

N. Ishimura and R. Arakaki contributed equally to this paper.
The online version of this article contains supplemental material.

The Rockefeller University Press $30.00
J. Exp. Med. Vol. 205 No. 12 2915-2927
www.jem.org/cgi/doi/10.1084/jem.20080174

autoimmune diseases are often tissue specific and sometimes involve antibodies against a restricted set of antigens, thereby prompting us to accept this most simple explanation for the initiation of autoimmunity. The loss of local tolerance is considered to result from the combined effect of different environmental factors. MHC class II genes are constitutively expressed only on hematopoietic cells involved in antigen presentation (dendritic cells, macrophages, B cells, and cortical thymic epithelial cells), but can be aberrantly induced by inflammatory stimuli on many other cell types (such as endothelial cells, hepatocytes, β cells of the pancreas, and thyrocytes) (12, 13). Although it has been implicated in allograft rejection (14), and subsequently in autoimmunity, it is still unknown whether to initiate autoimmunity class II molecules have to be expressed on professional APCs within secondary lymphoid organs or on nonhematopoietic cells of the target organ itself.

It has been suggested that estrogenic action is responsible for the strong female preponderance of many autoimmune diseases, including systemic lupus erythematosus (SLE), rheumatoid arthritis (RA), and Sjögren's syndrome (SS) (15, 16). Recent evidence suggests that apoptosis plays a key role in the physiology and pathogenesis of various autoimmune diseases, including SS (17–21). We have demonstrated that estrogenic action influences target epithelial cells through Fas-mediated apoptosis in a murine model for SS (21). Recently, we found that tissue-specific apoptosis in the exocrine glands spontaneously occurring in estrogen-deficient mice may contribute to the development of autoimmune exocrinopathy (22). Searching for the role of estrogen deficiency in the development of autoimmunity, we have recently identified retinoblastoma-associated protein 48 (RbAp48) gene specific for estrogen deficiency–dependent apoptosis in the exocrine glands, and transgenic expression of RbAp48 gene induced tissue-specific apoptosis in the exocrine glands (23). In this transgenic mouse model, we propose a possible clear and defined ab initio relationship between aberrant exposure of MHC class II molecules on IFN-γ–producing epithelial cells and disease development (i.e., autoimmune exocrinopathy).

RESULTS

Autoimmune exocrinopathy develops in *RbAp48*-transgenic (Tg) mice

We have generated *RbAp48*-Tg mice where the RbAp48 gene is expressed in the salivary and lacrimal glands using the salivary gland–specific promoter (23). When the histopathology of all organs from those mice were analyzed, we found that autoimmune exocrinopathy resembling SS developed in almost all *RbAp48*-Tg mice at 24 wk of age or more, but not in the WT mice. Lymphocyte infiltration in salivary and lacrimal glands of *RbAp48*-Tg mice becomes more frequent at ~30–50 wk of age (Fig. 1 A), and a significantly higher incidence of inflammatory lesions was found in female Tg mice at all ages (not depicted). Many infiltrating lymphocytes were observed in periductal areas at moderate (score 2) to severe (score 4) degrees, and shown in focal appearance. Representative histopathological features of the inflammatory lesions in lachrymal and salivary (submandibular) glands from *RbAp48*-Tg mice were shown in Fig. 1 B. No inflammatory lesions were observed in other organs of *RbAp48*-Tg mice. A majority of infiltrating cells in salivary and lacrimal glands were Thy1.2$^+$ CD4$^+$ T cells, whereas a minor proportion of B220$^+$ B cells, CD8$^+$ T cells (Fig. 1 C), and CD11b$^+$ cells (unpublished data) was observed. When the function of lacrimal and salivary glands in *RbAp48*-Tg mice was analyzed, the mean volume of tear and saliva secretion from *RbAp48*-Tg mice was significantly lower than that from the WT group at 30 wk of age or more (Fig. 1 D). Regarding the peripheral T cell phenotype of *RbAp48*-Tg mice, T cell activation markers (CD44^{high}, CD62L^{low}, CD45RB^{low}) were up-regulated on CD4$^+$ T cells in cervical LNs (cLNs) from *RbAp48*-Tg mice, compared with those from WT mice (Fig. 2 A). No significant difference was observed in thymic T cells gated on CD4$^+$CD8$^-$ bearing CD69, CD25, and CD62L^{low} between Tg and WT mice (Fig. S1, available at http://www.jem.org/cgi/content/full/jem.20080174/DC1). As for the phenotype of CD4$^+$CD25$^+$Foxp3$^+$ T reg cells, no difference

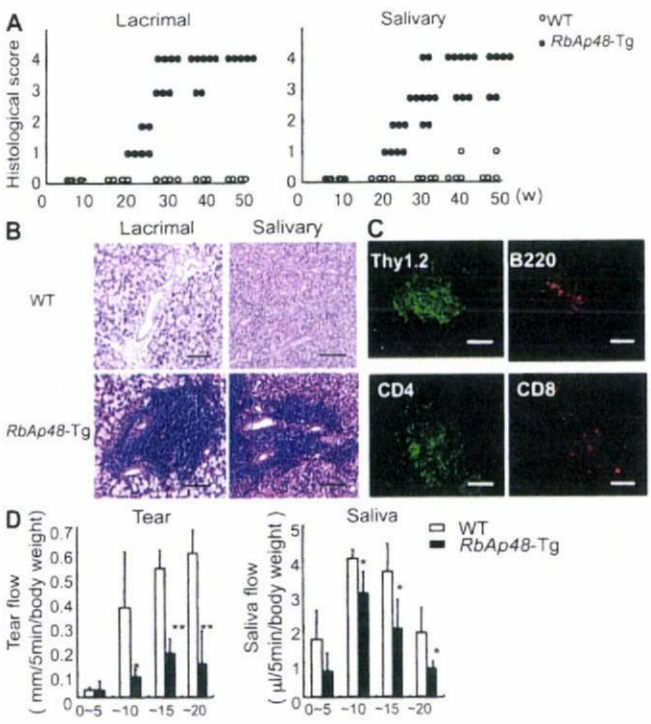

Figure 1. Autoimmune lesions in *RbAp48*-Tg mice. (A) Mean grade of inflammatory lesions in salivary and lacrimal glands from WT and *RbAp48*-Tg mice 10–50 wk of age. (B) Images (H&E staining) are representative of 5–7 mice at 32 wk of age. (C) Lymphocyte populations of the salivary gland lesion from *RbAp48*-Tg mice at 24 wk of age. Thy1.2$^+$, CD4$^+$, CD8$^+$ T cells, or B220$^+$ B cells were detected by immunofluorescence staining with FITC- (green) or PE-conjugated (red) mAbs using the frozen sections. Images are representative of three to five samples from each group. (D) The mean volume of saliva and tear secretion from WT and *RbAp48*-Tg mice at 30 wk of age was measured. Data are means ± SE of five mice. The results are representative of two independent experiments. Bars: (B) 100 μm; (C) 40 μm.

was detected in thymus, spleen, and cLNs between *RbAp48*-Tg and WT mice (Fig. S2). Moreover, culture supernatants from anti–TCR-β and -CD28 mAb-stimulated cLN T cells obtained from *RbAp48*-Tg mice contained higher levels of IL-2 and IFN-γ, whereas no difference in IL-4 and -10 levels between *RbAp48*-Tg and WT mice was observed by ELISA (Fig. 2 B). Our previous reports identified a 120-kD α-fodrin as an important autoantigen in murine and human SS (24, 25). It is particularly interesting that a higher titer of serum autoantibodies against SS-A (Ro), SS-B (La), and 120-kD α-fodrin was detected in *RbAp48*-Tg mice, compared with that in WT mice by ELISA (Fig. 2 C). This result is consistent with the characteristic flow cytometric finding that showed a significant $CD5^+B220^+$ fraction capable of autoantibody production (26) that appeared in spleen cells from *RbAp48*-Tg mice compared with WT mice (Fig. 2 D). On the other hand, the $CD5^+B220^+$ cells were undetectable in both salivary and lacrimal glands from *RbAp48*-Tg mice (Fig. S3 A). In addition, significantly increased $CD21^{high}IgM^{high}B220^+$ marginal zone B cells were observed in both cervical lymph nodes and spleen from *RbAp48*-Tg mice compared with those from WT mice (Fig. S3). These results may provide a new animal model for autoimmune exocrinopathy resembling SS, which should help us to further understand how autoreactive T cells are developed, and subsequently influence the development of autoimmunity.

Salivary gland epithelial cells function as APCs

It is well known that nonlymphoid cells that express MHC class II molecules provoke autoimmune responses (12, 13). However, it is undetermined whether MHC class II–expressing epithelial cells can function as APCs. We frequently observed MHC class II molecule expression on the exocrine gland cells in *RbAp48*-Tg mice, but not in WT mice (Fig. 3 A). These molecules play a pivotal role in the induction and regulation of immune responses by virtue of their ability to present self-peptides to $CD4^+$ T cells (27). To examine whether salivary epithelial cells could act as APCs, mouse salivary gland (MSG) cells, splenocytes, and splenic $CD11c^+$ DCs from *RbAp48*-Tg mice and WT mice were compared in terms of their capacity to express MHC class II and costimulatory molecules, including CD86, CD80, and ICAM-1, by flow cytometric analysis. Among them, a considerably large proportion of MHC class II^+, $CD86^+$ cells, $CD80^+$ cells, and $ICAM\text{-}1^+$ cells was observed on MSG cells from Tg mice, compared with those from WT mice (Fig. 3 B). MSG cells

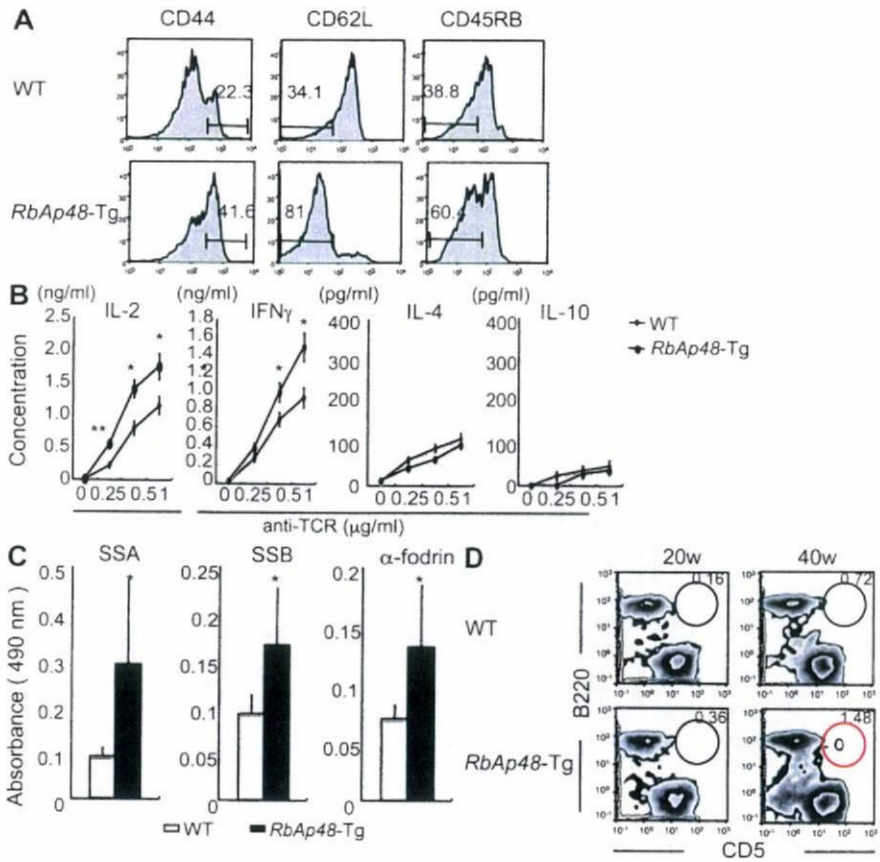

Figure 2. Immune responses in *RbAp48*-Tg mice. (A and B) Activation markers and cytokine production of $CD4^+$ T cells of cLNs from WT and *RbAp48*-Tg mice at 32 wk of age. (C) Autoantibodies of sera from *RbAp48*-Tg mice at 28–32 wk of age. (D) $CD5^+B220^+$ population of spleen from *RbAp48*-Tg and WT mice at 20 and 40 wk of age was analyzed by flow cytometry. Results are representative of means ± SE of five to seven mice in three independent experiments. *, $P < 0.05$; **, $P < 0.005$; WT versus *RbAp48*-Tg mice.

were enriched by enzymatic treatment and using several antibodies against immune cells, epithelial cells, and magnetic beads, as shown in Fig. S4 A (available at http://www.jem.org/cgi/content/full/jem.20080174/DC1). DCs were undetectable in the purified MSG cell suspension (Fig. S4 B). On the other hand, although the expressions of MHC class II and CD86 on the splenocytes and CD11c$^+$ DCs were higher than those on both MSG cells, the expressions of CD80 and ICAM-1 on the professional APCs were similar or lower than those on the MSG cells (Fig. 3 B). These expressions (MHC class II$^+$, CD86$^+$, CD80$^+$, and ICAM-1$^+$) on salivary epithelial cells from *RbAp48*-Tg mice were also confirmed by confocal analysis (Fig. 3 C). Controls using isotype antibodies for immunostainings were shown in Fig. S4 B. Moreover, to examine whether the peripheral T cells from *RbAp48*-Tg mice can respond to the MSG cells that show phenotypes for the APCs, CFSE-labeled purified CD4$^+$ (10^5) T cells from *RbAp48*-Tg mice were co-cultured with the MSG cells (1 and 2×10^5) from those mice or WT mice. Although CD4$^+$ T cells from B6 mice could not respond to both B6 and *RbAp48*-Tg MSG cells, CD4$^+$ T cells from *RbAp48*-Tg mice were capable of responding to MSG cells from *RbAp48*-Tg mice, but not with those from WT mice, whereas anti–MHC class II antibody inhibits these responses (Fig. 4 A). Furthermore, proliferation assay using [^{3}H]thymidine incorporation demonstrated that purified CD4$^+$ T cells of cLNs from *RbAp48*-Tg mice were more proliferative to the MSG cells from *RbAp48*-Tg mice relative to those from WT mice (Fig. 4 B). Additionally, significantly increased proliferation of the CD4$^+$ T cells to peripheral DCs from *RbAp48*-Tg

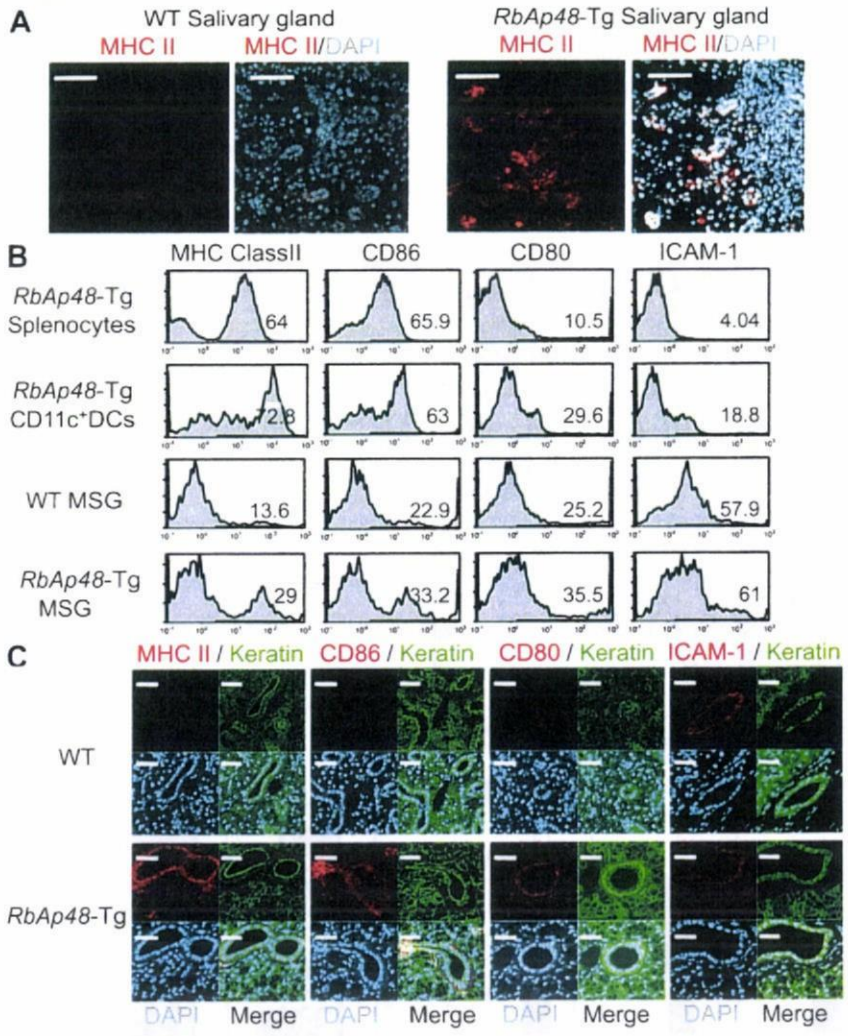

Figure 3. Antigen-presenting function in salivary epithelial cells. (A) MHC class II expression of salivary tissues from WT and *RbAp48*-Tg mice was detected by confocal analysis using anti–MHC class II mAb, Alexa Fluor 568–conjugated anti-rat IgG (red) and DAPI (blue). Images are representative of five to seven mice. (B) APC markers of splenocytes, splenic DCs, and MSG cells from WT and *RbAp48*-Tg mice were analyzed by flow cytometer. Results are representative of three to five mice in two independent experiments. (C) APC markers of MSG epithelial cells were detected by confocal analysis using anti–MHC class II, CD86, CD80, ICAM-1 mAbs, anti-keratin polyclonal antibody, Alexa Fluor 568–conjugated anti-rat IgG (red), Alexa Fluor 488–conjugated anti-rabbit IgG (green), and DAPI (blue). Images are representative of five to seven mice. Bars: (A and C) 50 µm.

mice was observed compared with DCs from WT mice (Fig. 4 C). Approximately half of the T cells response to 10^5 DCs from *RbAp48*-Tg mice equaled the level of the response to 10^5 MSG cells from the Tg mice (Fig. 4, B and C).

Crucial role of epithelial IFN-γ production

The expression of MHC class II molecules is generally regulated at the transcriptional levels, including the transcription factor IFN regulatory factor (IRF)-1 (28, 29) and the class II transactivator (CIITA), which is the master regulator for MHC class II gene expression (30, 31). It has been shown that IRF-1 is a primary responsible gene of the IFN-γ response (32). In in vitro studies using human salivary gland (HSG) cells (33), IFN-γ–induced mRNAs of IRF-1 and CIITA were significantly enhanced by treatment with Tamoxifen (Tam), which is an antagonist of estrogen and can induce RbAp48 (23), or transfection of pCMV-*RbAp48* plasmid in the dose-dependent manner (Fig. 5 A), not in MCF-7 cells (human mammary gland cell line; Fig. S5, A and B, available at http://www.jem.org/cgi/content/full/jem.20080174/DC1). In addition, we next analyzed the IRF-1 promoter activity using *RbAp48*-transfected HSG cells with and without IFN-γ by luciferase assay. We observed significantly enhanced IRF-1 promoter activity in *RbAp48*-transfected HSG cells with IFN-γ, not in MCF-7 cells (Fig. 5 B). Surprisingly, in *RbAp48*-Tg mice, a prominent expression of IFN-γ was detected in salivary and lacrimal epithelial cells besides sporadically positive infiltrating cells of *RbAp48*-Tg mice, not WT mice (Fig. 5 C). These findings were observed mainly in the MHC class II^+ ductal epithelium adjacent to lymphoid infiltrates. Epithelial IFN-γ expression in the exocrine glands of *RbAp48*-Tg mice was up-regulated during the course of autoimmune exocrinopathy. Induction of IFN-γ expression may occur through many different types of stimulation, including cross-linking of cell-surface receptors and stimulation with cytokines, including IL-2, -12, and -18 (34). It has been demonstrated that IFN-γ synthesis is predominantly induced by stimulation with IL-18 (35). Consistent with a previous study (36), IL-18 expression was observed in salivary epithelial cells in *RbAp48*-Tg mice, not in WT mice (Fig. 5 D). Confocal analysis revealed that differential expression of IL-18 and IFN-γ was clearly observed, i.e., IL-18 mainly in the acinar cells and IFN-γ in the duct cells, within salivary epithelial cells from *RbAp48*-Tg mice, but not from WT mice (Fig. 5 D). Controls using isotype antibodies were shown in Fig. S4 C. Epithelial IFN-γ and IL-18 productions were confirmed by flow cytometry using MSG cells without immune cells from *RbAp48*-Tg, not from WT mice, whereas there was no difference in both IFN-γ and IL-18 expressions of cLN cells between WT and *RbAp48*-Tg mice (Fig. 5 E). Although the production of IL-18 in salivary gland cells was detected in a previous study (36), there has been no proof for IFN-γ production of salivary gland cells in any paper. Therefore, to confirm IFN-γ production of exocrine glands, detection of IFN-γ using tissue homogenates was performed. A high concentration of IFN-γ was detected in the tissue homogenates of lacrimal and salivary glands from *RbAp48*-Tg mice, compared with that from WT mice, by ELISA (Fig. S6 A). Furthermore, the detection of IFN-γ mRNA of MSG cells was performed by in situ hybridization using the RNA probe of mouse IFN-γ gene. A more intense signal for IFN-γ mRNA in duct cells of salivary glands from *RbAp48*-Tg mice was observed compared with that from WT mice (Fig. 5 F). As for the expression of BAFF, which is an inducer of IFN-γ in B cells, the expression of epithelial cells was undetectable in both *RbAp48*-Tg and WT mice (Fig. S7). In vitro studies using HSG cells demonstrated that the expressions of IL-18, IFN-γ, and MHC class II (HLA-DR) were observed

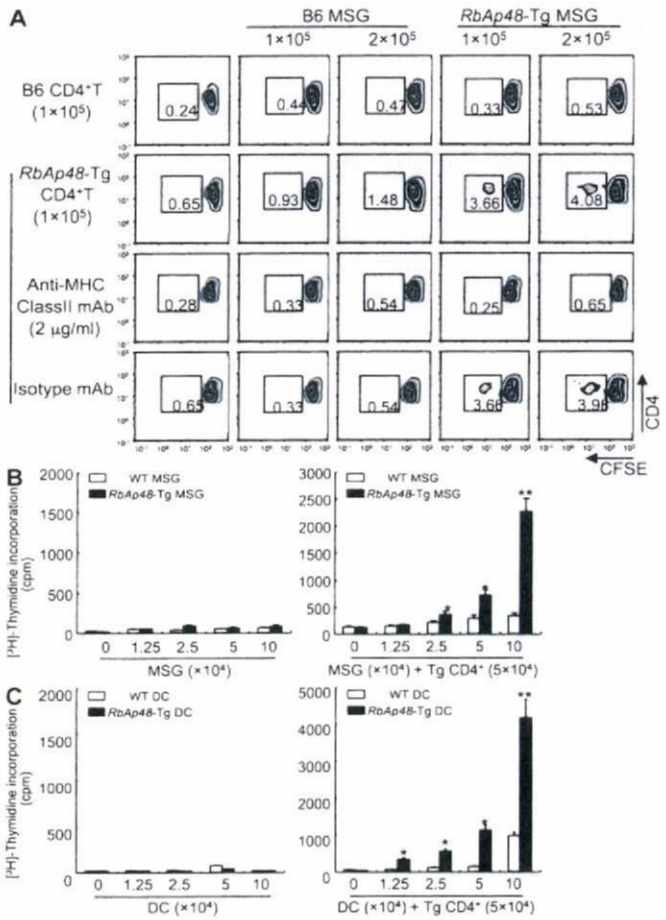

Figure 4. CD4⁺ T cells can proliferate to epithelial cells from *RbAp48*-Tg mice. (A) CFSE-labeled purified $CD4^+$ T cells (10^5) of WT and *RbAp48*-Tg mice were co-cultured with MSG cells (1 and 2 × 10^5) from the mice for 72 h. Cell proliferation was estimated by the dilution of CFSE. 2 μg/ml anti-MHC class II mAb or isotype control antibody was added in the culture. All results are representative of three to five mice at 28 wk of age, or three-independent experiments. (B) $CD4^+$ T cells (5 × 10^4) of cLNs from *RbAp48*-Tg mice were co-cultured with irradiated MSG cells (0–10 × 10^4) from WT and *RbAp48*-Tg mice for 72 h. (C) $CD4^+$ T cells (5 × 10^4) of cLNs from *RbAp48*-Tg mice were co-cultured with irradiated DCs (0–10 × 10^4) from WT and *RbAp48*-Tg mice for 72 h. Proliferative T cell response was evaluated by [^{3}H]thymidine incorporation during the last 12 h of the culture. Results are representative of means ± SE of triplicates in two independent experiments. *, $P < 0.05$; **, $P < 0.005$; WT versus *RbAp48*-Tg MSG cells or DCs.

when treated with Tam or transfected with pCMV-*RbAp48*, whereas they were inhibited when treated with 17β-estradiol (E2), caspase 1 inhibitor (Ac-YVAD-CHO; Ci), and siRNA of *RbAp48* (si; Fig. 6 A). Confocal analysis confirmed the expression of IL-18 and IFN-γ in HSG cells treated with Tam or transfected with pCMV-*RbAp48* (Fig. 6 B). It is important to note that IL-18 is secreted earlier (by 6 h) than IFN-γ production and HLA-DR expression (by 12 h) in Tam-stimulated and *RbAp48*-transfected HSG cells (Fig. S8). The most prominent function of IL-18 is its capacity to act as a potent costimulus for IFN-γ production (37–39). Indeed, we observed an increase in IFN-γ production in HSG cells treated with

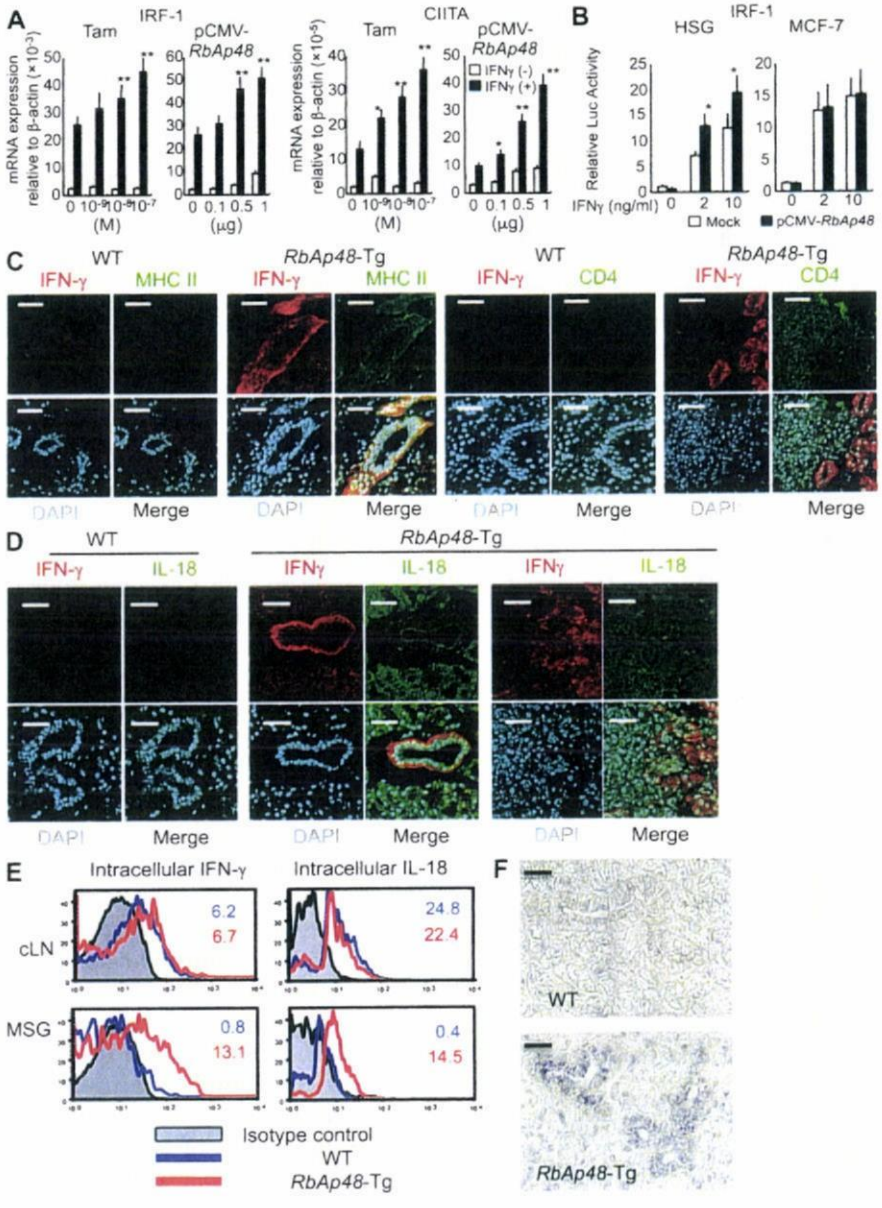

Figure 5. IFN-γ production from salivary epithelial cells stimulated with RbAp48. (A) IRF-1 and CIITA mRNA expressions of HSG cells stimulated with Tam (~10^{-9}–10^{-7} M) or transfected with pCMV-*RbAp48* (~0–1 μg) in the presence of IFN-γ (5 ng/ml) were detected by real-time PCR. Data are shown as means ± SE (SE) relative to β-actin mRNA of two independent experiments. *, $P < 0.05$; **, $P < 0.005$, versus IFN-γ (+) Tam 0 M or IFN-γ (+) pCMV-RbAp48 0 μg. (B) Promoter activity of IRF-1 in HSG and MCF-7 cells transfected with pCMV-*RbAp48*. Data are shown as means ± SE (SE) of two independent experiments. *, $P < 0.05$; **, $P < 0.005$, versus Mock (C and D) Confocal analysis of IFN-γ, MHC Class II, CD4, IL-18 or DAPI of salivary gland tissues from WT and *RbAp48*-TG mice at 32 wk of age. Alexa Fluor 488– or Alexa Fluor 568–conjugated anti-rat IgG were used as the second antibodies. Images are representative of three to five mice. (E) Intracellular IFN-γ and IL-18 expressions of cLN and MSG (without immune cells) cells from WT and *RbAp48*-Tg mice at 32 wk of age was detected by flow cytometric analysis. Results are representative and are shown as means ± SE of three mice of each group in two independent experiments. (F) The expression of IFN-γ mRNA in salivary gland cells of *RbAp48*-Tg mice was detected by in situ hybridization. Representative images of WT and *RbAp48*-Tg mice are shown in two independent experiments. Negative (antisense probe) or positive controls for mouse IFN-γ RNA probe are shown in Fig. S6 B. Fig. S6 is available at http://www.jem.org/cgi/content/full/jem.20080174/DC1. Bars: (C) 50 μm; (D) 40 μm.

recombinant IL-18 in the dose-dependent manner, but not in MCF-7 cells (Fig. S9, available at http://www.jem.org/cgi/content/full/jem.20080174/DC1), by ELISA and flow cytometry (Fig. 6 C). Confocal analysis of IFN-γ production of HSG cells in response to IL-18 together with cytokeratin as an identified marker was shown in Fig. 6 D. Moreover, we found a significant up-regulation of caspase 1 activity in lacrimal and salivary glands from *RbAp48*-Tg mice relative to that from WT mice (Fig. 6 E). In this regard, we reported previously significantly increased caspase 1 activity in salivary gland tissues from ovariectomized (Ovx) C57BL/6 mice in vivo (22) and Tam-stimulated and *RbAp48*-transfected HSG cells in vitro (23).

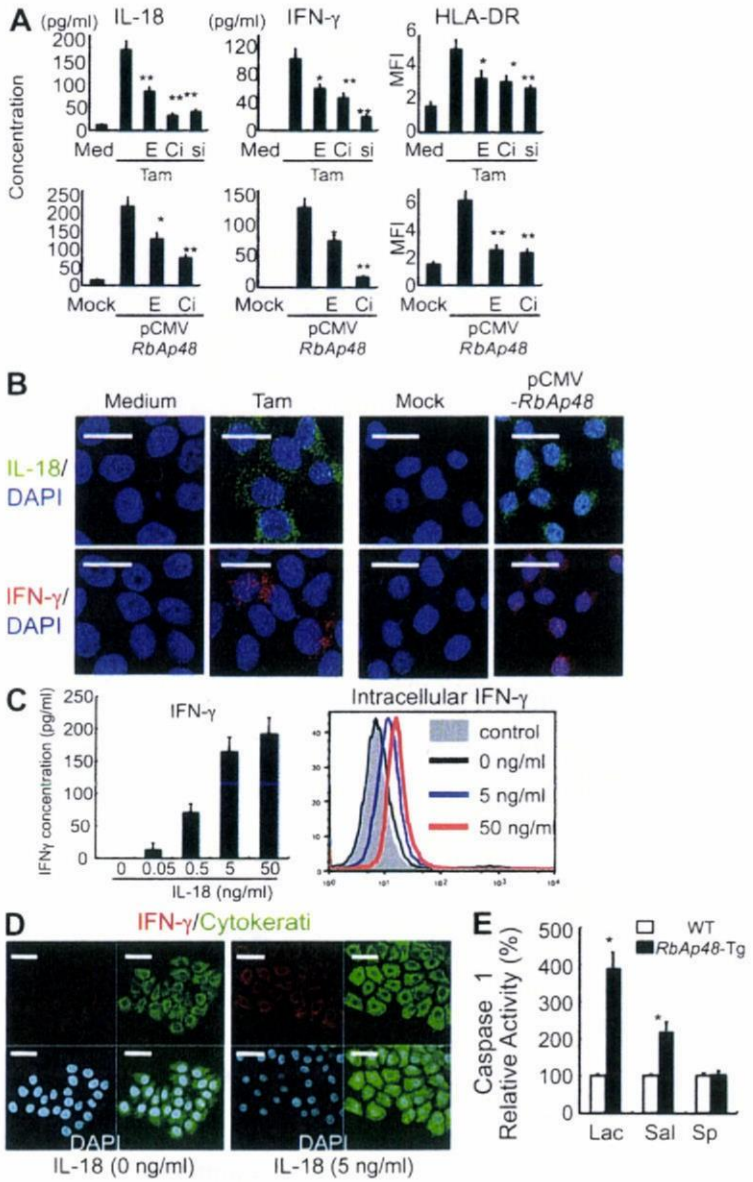

Figure 6. Expressions of IL-18, IFN-γ, and MHC class II (HLA-DR) in HSG cells when treated with Tam and transfected with pCMV-*RbAp48*. (A) Inhibitory effects of 10^{-9} M 17β-estradiol (E) or 10 μM caspase 1 inhibitor (Ci) on RbAp48-induced IL-18, IFN-γ, and HLA-DR in HSG cells. IL-18 and IFN-γ of the culture supernatants were detected by ELISA. HLA-DR is shown as mean fluorescence intensity (MFI) by flow cytometric analysis. *, $P < 0.05$; **, $P < 0.005$, versus RbAp48-induced. Data are means ± SD of triplicate samples, and representative of two independent experiments. (B) Tam- or RbAp48-induced IL-18 and IFN-γ were detected by confocal microscopic analysis. IL-18, IFN-γ mAbs, and Alexa Fluor 488– or Alexa Fluor 568–conjugated anti-mouse IgG were used. Images are representative of three independent experiments. (C) IFN-γ secretion or production of HSG cells by the addition of recombinant IL-18 was detected by ELISA or intracellular flow cytometric analysis. Data are representative of three independent experiments. (D) IFN-γ expression of IL-18–stimulated HSG cells was detected by confocal microscopic analysis together with cytokeratin and DAPI stainings. Images are representative of three independent experiments. (E) Caspase 1 activity of lacrimal, salivary glands, and spleen from *RbAp48*-Tg mice at 28 wk of age. Data are shown as means ± SE of four mice in two independent experiments, relative to those of WT mice. *, $P < 0.05$; **, $P < 0.005$; WT versus *RbAp48*-Tg mice. Bars: (B) 20 μm; (D) 50 μm.

Transfer of autoimmune exocrinopathy in *RbAp48*-Tg mice

Because thymic T cell abnormality could not be observed in *RbAp48*-Tg mice, it is speculated that there may be dysregulation of peripheral tolerance. To know the homeostatic expansion of peripheral T cells from *RbAp48*-Tg mice, we adoptively transferred CFSE-labeled CD4$^+$ T cells from *RbAp48*-Tg mice into irradiated syngeneic C57BL/6.Ly5.1 mice and analyzed them 7 d later. As a result, we observed more substantial cell division of the donor CFSE-labeled cLN CD4$^+$ T cells from *RbAp48*-Tg mice than that from WT mice (Fig. 7 A), indicating that T cells undergoing homeostatic proliferation may provide a basis for autoimmunity (40, 41). This suggests that elicitation of CD4$^+$ T cell–mediated autoreactivity against autoantigen could be the primary pathogenic process that leads to substantial homeostatic expansion. Futhermore, we succeeded in adoptive transfer of autoimmune lesions in the exocrine glands into *Rag2*$^{-/-}$ mice using cervical lymph node cells, but not spleen cells, from *RbAp48*-Tg mice (Fig. 7, B and C). Interestingly, these transferred lesions were extremely enhanced in estrogen-deficient *Rag2*$^{-/-}$ mice treated with ovariectomy (Ovx) compared with the lesions in Sham *Rag2*$^{-/-}$ mice (Fig. 7, D and F), suggesting that estrogen deficiency accelerates autoimmune exocrinopathy, as previously reported (21, 22). When we examined the adoptive

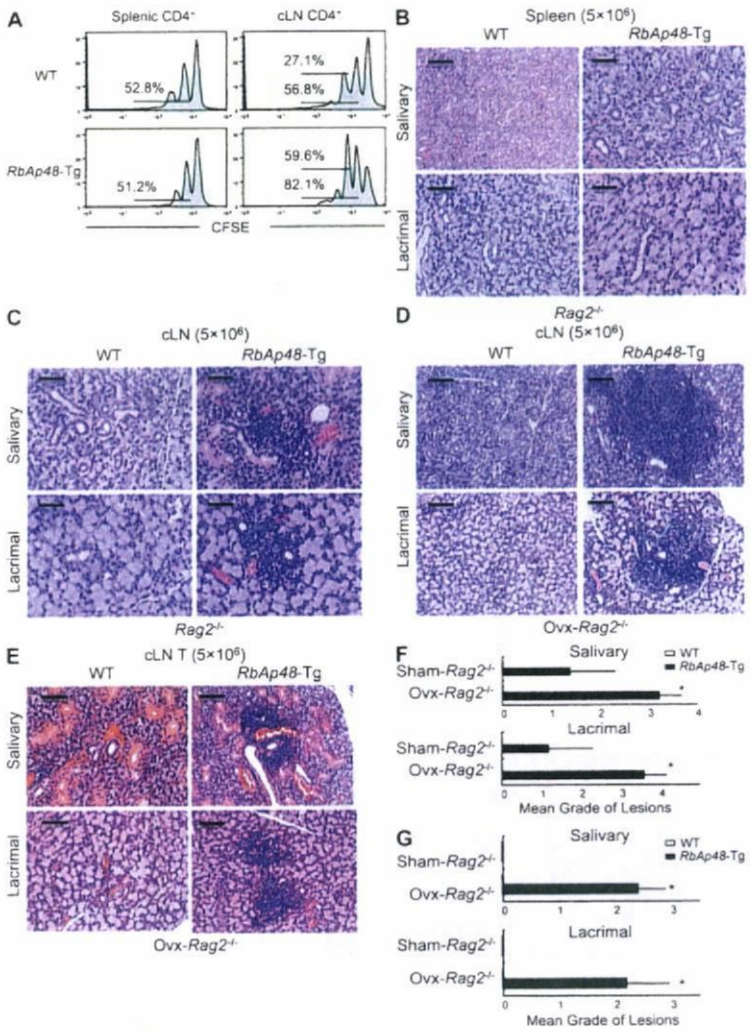

Figure 7. Transfer of autoimmune lesions from *RbAp48*-Tg mice into *Rag2*$^{-/-}$ mice. (A) Homeostatic proliferation of splenic and cLN T cells from WT and *RbAp48*-Tg mice at 28 wk of age was analyzed at 7 d after transfer into irradiated C57BL/6 mice. Results are representative of four to five mice in two independent experiments. Percentages of divided cells from the second or third division are indicated. (B and C) Spleen cells (5 × 10^6) or cLN cells (5 × 10^6) from WT and *RbAp48*-Tg mice at 30 wk of age were transferred into *Rag2*$^{-/-}$ mice. At 6 wk after the transfer, the pathology of salivary and lacrimal glands was analyzed. Images are representative of four to five mice. (D) cLN cells from WT and *RbAp48*-Tg mice were transferred into ovariectomized (Ovx) *Rag2*$^{-/-}$ mice. (E) T cells of cLNs from WT and *RbAp48*-Tg mice were transferred into ovariectomized (Ovx) *Rag2*$^{-/-}$ mice. Images of salivary and lacrimal gland tissues were representative of four to five mice. (F) Severity of inflammatory lesions of salivary and lacrimal glands from sham-operated (Sham) and Ovx-*Rag2*$^{-/-}$ hosts by transfer of cLN cells were shown as mean grade of lesions. (G) Severity of inflammatory lesions of salivary and lacrimal glands from sham-operated (Sham) and Ovx-*Rag2*$^{-/-}$ hosts by T cell transfer were shown as mean grade of lesions. Data are shown as means ± SE of four to five mice. *, $P < 0.05$, Sham versus Ovx. Bars: (B–E) 100 µm.

transfer using T cells isolated from cervical lymph nodes and spleen of *RbAp48*-Tg mice, no inflammatory lesions had developed in *Rag2*$^{-/-}$ mice (Table I). These data suggest that APCs besides T cells might be required for successful transfer of autoimmune exocrinopathy in *RbAp48*-Tg mice. Finally, to confirm that MHC class II expression on activated salivary or lacrimal gland cells of *RbAp48*-Tg mice can drive priming of purified T cells of cLNs from *RbAp48*-Tg mice to induce autoimmune lesions, the T cells of cLNs from *RbAp48*-Tg mice were transferred into Ovx-*Rag2*$^{-/-}$ mice. The autoimmune lesions of salivary and lacrimal glands from the recipient Ovx-*Rag2*$^{-/-}$ mice transferred with T cells of cLNs from *RbAp48*-Tg mice were observed, whereas no lesions were found in any organs of the recipient Ovx-*Rag2*$^{-/-}$ mice transferred with T cells of cLNs from WT mice (Fig. 7, E and G). These results demonstrate that the epithelial cells stimulated through increased RbAp48 because of estrogen deficiency could interact with T cells to induce autoimmunity via loss of local tolerance.

Table I. Induction of autoimmune lesions

Donor cells	Mice	Incidence
Spleen cells (5×10^6)	WT	0/4
	RbAp48-Tg	0/4
cLN cells (5×10^6)	WT	0/5
	RbAp48-Tg	4/5
cLN T cells (5×10^6)	WT	0/4
	RbAp48-Tg	0/5
cLN B cells (5×10^6)	WT	0/4
	RbAp48-Tg	0/4

Whole spleen, cLN cells, cLN T cells, or cLN B cells were transferred intravenously into *Rag2*$^{-/-}$ mice. The host mice were killed 6 wk after transfer. Inflammatory lesions of salivary or lacrimal glands were evaluated by pathological analysis.

IFN-γ and IL-18 expressions in human SS patients

Although it has been reported that immune cells express some cytokines, it is unclear whether IFN-γ or IL-18 together with RbAp48 in the epithelial cells of salivary glands from human SS patients are expressed. To confirm our hypothesis that autoimmunity is induced by a breakdown of local tolerance in salivary gland cells with up-regulated RbAp48 because of estrogen deficiency such as menopause, IFN-γ, IL-18, and RbAp48 expressions were detected by confocal microscopic analysis using human biopsy samples from SS patients and controls. Among 10 SS patients, RbAp48$^+$ and IFN-γ$^+$ epithelial cells were observed in three samples and RbAp48$^+$ and IL-18$^+$ epithelial cells were observed in four samples. A representative image of SS patients and controls is shown in Fig. 8. Although faint expressions of RbAp48 in the nucleus of salivary epithelial cells were detected in control samples, IL-18 or IFN-γ together with a prominent expression of RbAp48 was not observed (Fig. 8). Isotype-matched controls of staining for the mAbs were shown in Fig. S10 (available at http://www.jem.org/cgi/content/full/jem.20080174/DC1).

DISCUSSION

Although MHC class II molecules have been expressed aberrantly on epithelial cells in association with autoimmunity, it remains debatable whether class II molecules are the initiating event or the consequence of the autoimmune attack. For example, certain alleles of class II (mouse I-A^{g7}) might be particularly good at presenting glutamic acid decarboxylase–65 or insulin peptides to T cells in nonobese diabetic (NOD) mice, thus contributing to recognition and ultimate destruction of pancreatic β cells (10, 11). Some investigators have proposed that I-A^{g7}, because of its poor peptide-binding properties, enhances autoimmunity in NOD mice in a global fashion (42). In this case, the β cell specificity of autoimmunity in this strain and the switch to autoimmune thyroiditis when a class II molecule without these properties is exchanged for I-A^{g7} must be controlled by other genetic loci in NOD mice (43). It is possible that the most straightforward explanation for the effects of I-A^{g7} is that it predisposes to

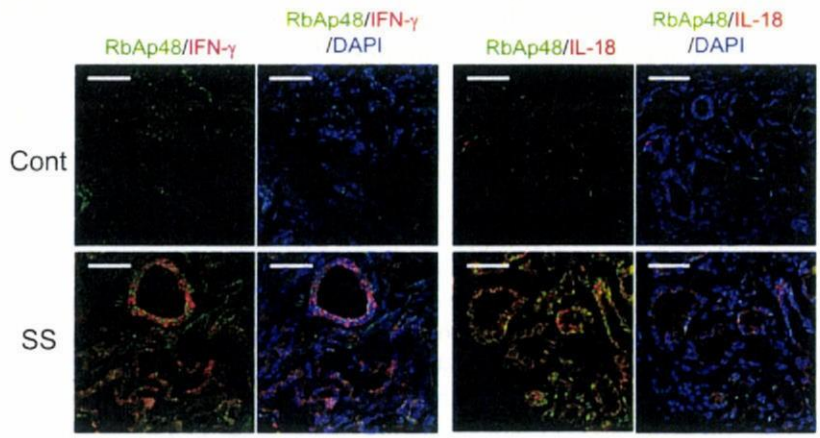

Figure 8. IFN-γ and IL-18 expressions together with RbAp48 in salivary glands from SS patients. The frozen sections of salivary glands from SS patients and controls were stained with IFN-γ or IL-18 (Alexa Fluor 568; red) and RbAp48 (Alexa Fluor 488; green) mAbs. The nuclei were stained with DAPI. The representative images in controls and SS patients were shown in three independent experiments.

islet-specific autoimmunity and not system-wide reactivity. Another piece of evidence that the role of MHC class II is antigen-specific is that the class II alleles predisposing toward autoimmunity vary in one human disease to another, indicating that class II alleles act in autoimmunity via specific antigens rather than comprehensively.

We demonstrated in this study that autoimmune exocrinopathy resembling SS developed in almost all *RbAp48*-Tg mice, and that a high titer of serum autoantibodies against SS-A (Ro), SS-B (La), and 120-kD α-fodrin was detected in these Tg mice. We frequently found MHC class II molecule expression on the exocrine gland cells with autoimmune lesions in *RbAp48*-Tg mice. When we examined whether salivary epithelial cells could act on antigen presentation, we found a large proportion of MHC class II^+, $CD86^+$, $CD80^+$, and ICAM-1^+ cells primarily observed on cultured MSG cells from Tg mice. Moreover, CFSE-labeled purified $CD4^+$ (10^5) T cells from *RbAp48*-Tg mice were capable of responding to MSG cells from *RbAp48*-Tg mice, whereas anti–MHC class II antibody inhibited these responses. Although it has not been determined whether MHC class II–expressing epithelial cells can function as APCs, those data strongly suggest that the epithelial cells may function as APCs during development of autoimmune exocrinopathy. In *RbAp48*-Tg mice, a surprisingly prominent expression of epithelial IFN-γ was detected beside sporadically positive infiltrating cells. These findings were observed mainly in the MHC class II^+ ductal epithelium adjacent to lymphoid infiltrates. Epithelial IFN-γ expression in the exocrine glands of *RbAp48*-Tg mice was up-regulated during the course of autoimmune exocrinopathy. A previously unknown, multifaceted role of IFN-γ as regulator of the local immune system, which is termed here local tolerance, is disclosed. As to the mechanism of CIITA induction in *RbAp48*-Tg mice, our findings demonstrate the essential role of RbAp48-driven stimulation of IFN-γ production and signaling leading to up-regulation of IRF-1 and CIITA. RbAp48, initially identified as retinoblastoma-binding proteins (44), was characterized as a component of distinct nucleosome-modifying complexes, including the nuclear histone deacetylases (45, 46). Although the functions of the RbAp48-like proteins in these complexes remain undetermined, it was reported that E2F-1 and RbAp48 are physically associated in the presence of Rb and histone deacetylase (47), suggesting that RbAp48 could be involved in transcriptional repression of E2F-responsive genes. Several reports have demonstrated that estrogen may play an inhibitory role on apoptosis in endothelial cells, breast cancer cells, cardiac myocytes, prostate cells, and neuronal cells (48–51). It has been shown that the transcription factor IRF-1 mRNA expression is induced by ICI 182,780 as an antiestrogenic reagent and repressed by estrogens in antiestrogen-sensitive cells (52). We demonstrated the first evidence that IFN-γ–producing epithelial cells in the exocrine glands function as APCs through the IRF-1–CIITA pathway, resulting in the development of autoimmune exocrinopathy via loss of local tolerance. SS is known to have the most female predominance of >95% among all the autoimmune patients (15, 16). One of the key questions in respect to the pathophysiology of autoimmune diseases is how autoreactivity to particular autoantigens is initiated and maintained under an estrogen-deficient state. Although an important role for T cells in the development of autoimmune disease has been argued (53, 54), it is not known if disease is initiated by a retrained inflammatory reaction to autoantigen. We clarified that epithelial IFN-γ production is crucial for the initiation of autoimmune reactions between epithelial cells and autoreactive T cells with homeostatic expansion. Our previous study suggests that antiestrogenic actions have a potent effect on the proteolysis of α-fodrin autoantigen in the salivary gland through up-regulation of caspase 1 activity (22). These results strongly suggest that RbAp48-mediated activation of caspase 1 leads to the cleavage and activation of IL-18, which may act directly on IFN-γ production and on effector $CD4^+$ T cells by inducing migration and proliferation. Thus, aberrant expression of MHC class II in the exocrine glands facilitates loss of local tolerance before the development of autoimmune lesions, which is very similar to SS.

Evidence has been mounting that estrogen deficiency such as menopause is a proinflammatory state, which promotes osteoporosis and atherosclerosis, as well as autoimmunity (55, 56). In vivo and in vitro experiments here, including the induction of autoimmune lesions by T cell transfer from *RbAp48*-Tg mice into Ovx-*Rag2*$^{-/-}$ mice and in vitro antigen presentation of the Tg MSG cells to $CD4^+$ T cells, strongly suggests that estrogen deficiency stimulates salivary epithelial cells that are activated via the up-regulation of RbAp48 to present any endogenous autoantigen to $CD4^+$ T cells for the onset of autoimmune lesion in the salivary glands resembling human SS. Our data finds that transfer of cLN T cells from *RbAp48*-Tg mice into Ovx-*Rag2*$^{-/-}$ mice leads to autoimmune lesions, consistent with the conclusion that estrogen deficiency leads to the ability of salivary gland epithelial cells to express MHC class II and present any self-antigens. Most importantly, the salivary gland cells from human SS patients express RbAp48 together with IFN-γ or IL-18, as well as the findings of *RbAp48*-Tg mice in this work, suggesting that the molecules would be useful for any clinical application.

Collectively, our results demonstrate a direct molecular mechanism by which estrogen deficiency induces tissue-specific overexpression of RbAp48 (23), subsequently developing $CD4^+$ T cell–mediated autoimmunity through epithelial IFN-γ production. Thus, reducing the RbAp48 overexpression is a possible effective therapy in gender-based autoimmune exocrinopathy.

MATERIALS AND METHODS

Mice and histology. *RbAp48*-Tg mice have been previously described (23), and the RbAp48 gene is regulated by lacrimal and salivary gland–specific promoter (57). *Rag2*$^{-/-}$ mice were obtained from Taconic. All mice were reared in our specific pathogen–free mouse colony, and given food and water ad libitum. The experiments were approved by an animal ethics board of Tokushima University. All organs were removed from the mice, fixed with 4% phosphate-buffered formaldehyde (pH 7.2), and prepared for

histological examination. Formalin-fixed tissue sections were subjected to hematoxylin and eosin (H&E) staining, and three pathologists independently evaluated the histology without being informed of the condition of each individual mouse. Histological grading of the inflammatory lesions was done according to the method proposed by White and Casarett (58), as follows: 1 = 1–5 foci composed of >20 mononuclear cells per focus, 2 = >5 such foci, but without significant parenchymal destruction, 3 = degeneration of parenchymal tissue, and 4 = extensive infiltration of the glands with mononuclear cells and extensive parenchymal destruction. Histological evaluation of the salivary and lacrimal glands was performed in a blind manner, and a tissue section from each salivary and lacrimal gland was examined.

Measurement of fluid secretion. Analysis of the tear and saliva volume of WT and *RbAp48*-Tg mice was performed according to a previously described method (59).

Flow cytometric analysis. Lymphocytes in spleen, cLN, thymus, and MSG epithelial cells without immune cells (>95% of cells were keratin$^+$) were prepared. Surface markers were identified by mAbs with an EPICS flow cytometer (Beckman Coulter). Rat mAbs to FITC-, PE-, or PE-Cy5–conjugated anti-B220, CD4, MHC class II, CD86, CD80, ICAM1, and CD5 mAbs (eBioscience) were used. Appropriate isotype-matched controls were used, respectively. For detection of T cell activation markers, FITC-conjugated anti-CD25, CD44, CD62L, CD45RB, and CD69 mAbs (eBioscience) were used. Intracellular Foxp3 expression with an Intracellular Foxp3 Detection kit (eBioscience) was performed according to the manufacturer's instructions. Detections of intracellular IFN-γ or IL-18 were also performed by the same procedure. The data were analyzed with FlowJo FACS Analysis software (Tree Star, Inc.).

ELISA. The amount of mouse IL-2, IFN-γ, IL-4, and IL-10 in culture supernatants from CD4$^+$ T cells stimulated with anti-TCR mAb (~0–1 μg/ml) and anti-CD28 mAb (20 μg/ml; eBioscience), anti-SSA, anti-SSB, and anti–α-fodrin autoantibodies of sera from WT and *RbAp48*-Tg mice and human IL-18 and IFN-γ from cultured HSG and MCF-7 cells were analyzed by ELISA. In brief, plates were coated with a capture antibody or recombinant proteins (SSA, SSB, and α-fodrin), and washed with PBS/0.1% Tween 20. The plates were incubated with diluted culture supernatants or sera. After washing with PBS/0.1% Tween 20 and incubation of biotin-conjugated antibodies for cytokine detection, a horseradish peroxidase–conjugated detection antibody for autoantibody detection was added. After incubation with streptavidin-horseradish peroxidase for cytokine detection, plates were again washed with PBS/0.1% Tween 20 and o-phenylendiamine (Sigma-Aldrich) buffer added. Plates were then analyzed with a microplate reader reading at 490 nm.

Confocal microscopic analysis. Confocal microscopic analysis using anti-Thy1.2, B220, CD4, CD8, MHC class II, IFN-γ, CD4 (eBioscience), keratin (LSL CO., LTD), and IL-18 (MBL) antibodies was performed on the frozen sections of salivary glands from WT and *RbAp48*-Tg mice, and on the cultured cells using Confocal Laser Microscan (LSM 5 PASCAL; Carl Zeiss, Inc.). As the second antibodies, Alexa Fluor 488 anti–mouse IgG (H+L), Alexa Fluor 568 goat anti–rabbit IgG (H+L), Alexa Fluor 488 donkey anti–rat IgG (H+L), Alexa Fluor 488 chicken anti–goat IgG (H+L), and Alexa Fluor 568 rabbit anti–goat IgG (H+L; Invitrogen) were used. The nuclear DNA was stained with DAPI (Invitrogen).

Cell culture. For the co-culture of MSG with CD4$^+$ T cells, MSG cells were prepared by digestion of collagenase and hyaluronidase, and CD11c$^+$, CD11b$^+$, B220$^+$, NK1.1$^+$, and Thy1.2$^+$ cells were removed by the mAbs and magnetic bead–conjugated anti–rat IgG (Invitrogen). CD4$^+$ T cells from cLNs were purified by mAbs (anti-MHC class II, CD8, CD11b, CD11c, B220, and NK1.1) and magnetic bead–conjugated anti–rat IgG. CFSE-labeled CD4$^+$ T cells were co-cultured with MSG cells for 72 h. Cell division of CD4$^+$ T cells was analyzed by dilution of CFSE through flow cytometry.

As for the co-culture with DCs or MSG cells, DCs from *RbAp48*-Tg or WT mice were enriched using DC collection kit (Invitrogen). After DCs or MSG cells were irradiated (9 Gy), purified CD4$^+$ T cells of cLNs from RbAp48-Tg mice were co-cultured with the DCs or MSG cells for 72 h. The T cells were then pulsed with 0.5 μCi [^{3}H]thymidine per well for the last 12 h of the culture. [^{3}H]thymidine incorporation was evaluated using an automated β liquid scintillation counter. HSG and MCF-7 cells were cultured in DME containing 10% FBS at 37°C. Tam (Wako Pure Chemical), 17β-estradiaol (Wako), 10 μM caspase 1 inhibitor (Sigma-Aldrich), and recombinant human IFN-γ (R&D Systems) were used for cell cultures. RbAp48 gene inserted into pCMV (2N3T) construct (a gift from D. Trouche, Centre National de la Recherche Scientifique, University of Tolouse, Tolouse, France) (47) was transfected into the cells using FuGENE6 Transfection Reagent (Roche). Small interfering RNA (siRNA) corresponding to coding sequence +136 to +156 of RbAp48 gene was synthesized by Hokkaido System Science: CGAGGAAUACAAAAUAUGGTT (sense), CCAUAUUUUGUAUUCCUCGTT (antisense). When the siRNA was transfected into HSG cells together with GFP plasmid, 73.4% of cells were found to be GFP$^+$ HSG cells by flow cytometric analysis. Furthermore, the relative protein expression of RbAp48 to β-actin was reduced to ~80% by the siRNA.

Real-time quantitative RT-PCR. Total RNA was extracted from cultured HSG and MCF-7 cells using ISOGEN (Wako Pure Chemical), and reverse transcribed. Transcript levels of IRF-1, CIITA, and β-actin were performed using PTC-200 DNA Engine Cycler (Bio-Rad Laboratories) with SYBR Premix Ex Taq (Takara). Primer sequences were as follows: IRF-1, forward 5′-ACCCTGGCTAGAGATGCAGA-3′ and reverse 5′-CCTTTTCCCCTGCTTTGTATCG-3′; CIITA, forward 5′-CAGGCAGCAGAGGAGAAGTTCACCATC-3′ and reverse 5′-CCGTGAGGATCCGCACCAGTTTGGGG-3′; β-actin, forward 5′-AAATCTGGCACCACACCTTC-3′ and reverse 5′-GAGGCGTACAGGGATAGCA-3′.

Caspase activity. Caspase activities were assayed using Caspase-Family Colorimetric Substrate Set (BioVision, Inc.). In brief, 100 μg cytoplasmic lysates from lacrimal glands, salivary glands, and spleen of WT and *RbAp48*-Tg mice were incubated with 200 μM Ac-YVAD-pNA (Caspase 1 substrate), at 37°C for 1 h. The absorbance of samples was read at 405 nm in a microplate reader.

Promoter assay. For the measurement of the transcriptional activity of IRF-1, IRF-1 luciferase reporter vector (IRF-1/Luc) was purchased from Panomics. HSG cells plated in a 48-well plate were transiently transfected with 0.1 μg of IRF-1/Luc and 0.1 μg of pCMV-*RbAp48* or mock plasmid and 0.05 μg of phRL-TK (Promega Corp.) as an internal control using the FuGENE6. The cells were incubated overnight and subsequently treated with IFN-γ. After 10 h, the cells were harvested and subjected to a luciferase assay by using a dual-luciferase reporter assay system (Promega Corp.) as per the manufacturer's instructions. Relative luciferase activity was expressed as the fold- increase relative to the activity of untreated controls after normalization to the relative background of Renilla luciferase activity.

Cell transfer. CFSE-labeled splenic and cLN T cells (5 × 10^6) from WT and *RbAp48*-Tg mice were intravenously transferred into irradiated (700 cGy) C57BL/6.Ly5.1 mice. On the seventh day after the transfer, spleen cells were analyzed to measure homeostatic proliferation via CFSE dilution by flow cytometry. For induction of autoimmune lesions, total cells, T cells, or B cells from spleen cells (5 × 10^6) or cLN cells (5 × 10^6) from WT and *RbAp48*-Tg mice were intravenously transferred into *Rag2*$^{-/-}$ mice. At 6 wk after the transfer, the pathology of all the organs, including salivary and lacrimal glands, was analyzed. In addition, *Rag2*$^{-/-}$ hosts were ovariectomized (Ovx) or sham operated (Sham). Adoptive cell transfer was performed on the next day after Ovx or Sham.

In situ hybridization. Mice were perfused transcardially with saline (0.9%) followed by 4% PFA. The salivary glands were collected and fixed in 4% PFA at 4°C for 3 h. 6 μm paraffin-embedded sections were prepared for ISH.

The RNA probe (587 bp) of mouse IFN-γ was produced by RT-PCR using primers (T3, AATTAACCCTCACTAAAGGGACTGGCAAAAGG-ATGGTGAC; T7, TAATACGACTCACTATAGGGAGATACAACCC-CGCAATCAC). Digoxigenin (DIG)-labeled antisense and sense control riboprobes were generated using DIG RNA labeling mix (Roche). The sections were pretreated with 10 μg/ml proteinase K for 10 min at room temperature and then hybridized with 1 μg/ml DIG-labeled probes at 45°C for 16 h. DIG was immunodetected with alkaliphosphatase-conjugated anti-DIG antibody. For positive controls, sections of spleen from lipopolysaccaride-injected mice were used. The probe was confirmed with the positive control sections, as shown in Fig. S6 B.

Human samples. Immunostaining for RbAp48 and IL-18 or IFN-γ were performed using lip biopsy samples from human SS patients and controls. All samples were obtained from the Tokushima University Hospital, Tokushima, Japan. This study was approved by certification of the ethics board of Tokushima University Hospital. All subjects signed a written informed consent before enrollment. All patients with SS were female, had documented xerostomia and keratoconjunctivitis sicca, and fulfilled the criteria of the Ministry of Health, Labor, and Welfare of Japan for the diagnosis of SS. All patients with SS had focus scores of greater than two in their lip biopsy and all tested positive for autoantibodies against Ro. Analysis was performed under the certification of the ethics board of Tokushima University Hospital. Frozen sections were stained with anti–human RbAp48 mAb (BD) and Alexa Fluor 488 donkey anti–mouse IgG (H+L; Invitrogen) and Biotin-conjugated anti–human IL-18 (MBL) or IFN-γ (eBioscience) mAbs and Alexa Fluor 568–conjugated streptavidin and analyzed by confocal microscopy. The nuclear DNA was DAPI.

Statistics. Student's *t* test was used for statistical analyses.

Online supplemental material. Fig. S1 shows T cell phenotypes of thymus from *RbAp48*-Tg and WT mice. Fig. S2 shows T reg cells of thymus, spleen, and cLN from *RbAp48*-Tg and WT mice. Fig. S3 shows B1 cells in salivary glands and marginal B cells of spleen and cLN from *RbAp48*-Tg and WT mice. Fig. S4 shows the purified MSG cells, and images of control staining for the expressions of MHC class II, CD86, CD80, ICAM-1, IFN-γ, and IL18. Fig. S5 shows IRF-1 and CIITA mRNA of MCF-7 cells stimulated with Tam or transfected with pCMV-*RbAp48*. Fig. S6 shows IFN-γ concentration of tissue homogenates of lacrimal, salivary, and spleen from *RbAp48*-Tg and WT mice, and control sections for in situ hybridization of IFN-γ mRNA. Fig. S7 shows BAFF expression of salivary glands and spleen from *RbAp48*-Tg and WT mice. Fig. S8 shows the time courses of IL-18, IFN-γ, and HLA-DR expressions of HSG cells stimulated Tam or transfected with pCMV-*RbAp48*. Fig. S9 shows IFN-γ secretion from MCF-7 in response to IL-18. Fig. S10 shows control staining for RbAp48 expression together with IFN-γ or IL-18 in salivary glands from human SS patients and controls. The online supplemental material is available at http://www.jem.org/cgi/content/full/jem.20080174/DC1.

The authors thank Ai Nagaoka and Noriko Kino for their technical assistance; Kumio J. Tanaka, Mizue Yamanaka, and Shino Niki of OurGenic Co., Ltd. for analysis by in situ hybridization; and Prof. Noriaki Takeda for analysis of samples of human SS patients.

This work was supported in part by a Grant-in-Aid for Scientific Research (nos. 17109016, and 17689049) from the Ministry of Education, Science, Sport, and Culture of Japan, and from the Uehara Memorial Foundation.

The authors have no conflicting financial interests.

Submitted: 25 January 2008
Accepted: 15 October 2008

REFERENCES

1. Richardson, B. 2007. Primer: epigenetics of autoimmunity. *Nat. Clin. Pract. Rheumatol.* 3:521–527.
2. Schoenborn, J.R., and C.B. Wilson. 2007. Regulation of interferon-g during innate and adaptive immune responses. *Adv. Immunol.* 96:41–101.
3. Mathews, M.B., and R.M. Bernstein. 1983. Myositis autoantibody inhibits histidyl-tRNA synthetase: a model for autoimmunity. *Nature.* 304:177–179.
4. Matsumoto, I., A. Staub, C. Benoist, and D. Mathis. 1999. Arthritis provoked by linked T and B cell recognition of a glycolytic enzyme. *Science.* 286:1732–1735.
5. Streilein, J.W., G.A. Wilbanks, and S.W. Cousins. 1992. Immunoregulatory mechanisms of the eye. *J. Neuroimmunol.* 39:185–200.
6. Griffith, T.S., T. Brunner, S.M. Fletcher, D.R. Green, and T.A. Ferguson. 1995. Fas ligand-induced apoptosis as a mechanism of immune privilege. *Science.* 270:1189–1192.
7. Steinman, L. 1996. Multiple sclerosis. A coordinated immunological attack against myelin in the central nervous system. *Cell.* 85:299–302.
8. Hutchings, P., L. O'Reilly, N.M. Parish, H. Waldmann, and A. Cooke. 1992. The use of a non-depleting anti-CD4 monoclonal antibody to re-establish tolerance to cells in NOD mice. *Eur. J. Immunol.* 22:1913–1918.
9. Haskins, K., and M. McDuffie. 1990. Acceleration of diabetes in young NOD mice with a $CD4^+$ islet-specific T cell clone. *Science.* 249:1433–1436.
10. Nepom, G.T., and W.W. Kwok. 1998. Molecular basis for HLA-DQ associations with IDDM. *Diabetes.* 47:1177–1184.
11. Stratmann, T., V. Apostolopoulos, V. Mallet-Designe, A.L. Corper, C.A. Scott, I.A. Wilson, A.S. Kang, and L. Teyton. 2000. The $I\text{-}A^{g7}$ MHC class II molecule linked to murine diabetes is a promiscuous peptide binder. *J. Immunol.* 165:3214–3225.
12. Londei, M., J.R. Lamb, G.F. Bottazzo, and M. Feldmann. 1984. Epithelial cell expressing aberrant MHC class II determinants can present antigen to cloned human T cells. *Nature.* 312:639–641.
13. He, X.L., C. Radu, J. Sidney, A. Sette, E.S. Ward, and K.C. Garcia. 2002. Structural snapshot of aberrant antigen presentation linked to autoimmunity: the immunodominant epitope of MBP complexed with I-Au. *Immunity.* 17:83–94.
14. Dallman, M.J., and D.W. Mason. 1983. Induction of Ia antigens on murine epidermal cells during the rejection of skin allografts. *Transplantation.* 36:222–224.
15. Whitacre, C.C., S.C. Reingold, and P.A. O'Looney. 1999. A gender gap in autoimmunity. *Science.* 283:1277–1278.
16. Whitacre, C.C. 2001. Sex differences in autoimmune disease. *Nat. Immunol.* 2:777–780.
17. Apostolou, I., Z. Hao, K. Rajewsky, and H. von Boehmer. 2003. Effective destruction of Fas-deficient insulin-producing β cells in type 1 diabetes. *J. Exp. Med.* 198:1103–1106.
18. Lamhamedi-Cherradi, S.E., S.J. Zheng, K.A. Maguschak, J. Peschon, and Y.H. Chen. 2003. Defective thymocyte apoptosis and accelerated autoimmune diseases in $TRAIL^{-/-}$ mice. *Nat. Immunol.* 4:255–260.
19. Rathmell, J.C., and C.B. Thompson. 2002. Pathways of apoptosis in lymphocyte development, homeostasis, and disease. *Cell.* 109:S97–S107.
20. Stassi, G., and R. De Maria. 2002. Autoimmune thyroid disease: new models of cell death in autoimmunity. *Nat. Rev. Immunol.* 2:195–204.
21. Ishimaru, N., K. Saegusa, K. Yanagi, N. Haneji, I. Saito, and Y. Hayashi. 1999. Estrogen deficiency accelerates autoimmune exocrinopathy in murine Sjogren's syndrome through Fas-mediated apoptosis. *Am. J. Pathol.* 155:173–181.
22. Ishimaru, N., R. Arakaki, M. Watanabe, M. Kobayashi, M. Miyazaki, and Y. Hayashi. 2003. Development of autoimmune exocrinopathy resembling Sjogren's syndrome in estrogen deficient mice of healthy background. *Am. J. Pathol.* 163:1481–1490.
23. Ishimaru, N., R. Arakaki, F. Omotehara, K. Yamada, K. Mishima, I. Saito, and Y. Hayashi. 2006. Novel role of RbAp48 for tissue-specific estrogen deficiency-dependent apoptosis in the exocrine glands. *Mol. Cell. Biol.* 26:2924–2935.
24. Saegusa, K., N. Ishimaru, K. Yanagi, K. Mishima, R. Arakaki, T. Suda, I. Saito, and Y. Hayashi. 2002. Prevention and induction of autoimmune exocrinopathy is dependent on pathogenic autoantigen cleavage in murine Sjögren's syndrome. *J. Immunol.* 169:1050–1057.
25. Haneji, N., T. Nakamura, K. Takio, K. Yanagi, H. Higashiyama, I. Saito, S. Noji, H. Sugino, and Y. Hayashi. 1997. Identification of α-fodrin as a candidate autoantigen in primary Sjögren's syndrome. *Science.* 276:604–607.
26. Berland, R., and H.H. Wortis. 2002. Origins and functions of B-1 cells with notes on the role of CD5. *Annu. Rev. Immunol.* 20:253–300.

27. Germain, R.N. 1994. MHC-dependent antigen processing and peptide presentation: providing ligands for T lymphocyte activation. *Cell.* 76:287–299.
28. Giroux, M., M. Schmidt, and A. Descoteaux. 2003. IFN-γ-induced MHC class II expression: transactivation of class II transactivator promoter IV by IFN regulatory factor-1 is regulated by protein kinase C-α. *J. Immunol.* 171:4187–4194.
29. Hobart, M., V. Ramassar, N. Goes, J. Urmson, and P.F. Halloran. 1997. IFN regulatory factor-1 plays a central role in the regulation of the expression of class I and II MHC genes in vivo. *J. Immunol.* 158:4260–4269.
30. Ting, J.P., and J. Trowsdale. 2002. Genetic control of MHC class II expression. *Cell.* 109:S21–S33.
31. Wright, K.L., and J.P. Ting. 2006. Epigenetic regulation of MHC-II and CIITA genes. *Trends Immunol.* 27:405–412.
32. Elser, B., M. Lohoff, S. Kock, M. Giaisi, S. Kirchhoff, P.H. Krammer, and M. Li-Weber. 2002. IFN-γ represses IL-4 expression via IRF-1 and IRF-2. *Immunity.* 17:703–712.
33. Shirasuna, K., M. Sato, and T. Miyazaki. 1981. A neoplastic epithelial duct cell line established form an irradiated human salivary gland. *Cancer.* 48:745–752.
34. Howard, A.Y. 2006. Unravelling the pros and cons of interferon-γ gene regulation. *Immunity.* 24:506–507.
35. Nakanishi, K., T. Yoshimoto, H. Tsutsui, and H. Okamura. 2001. Interleukin-18 regulates both Th1 and Th2 responses. *Annu. Rev. Immunol.* 19:423–474.
36. Bombardieri, M., F. Barone, V. Pittoni, C. Alessandri, P. Conigliaro, M.C. Blades, R. Priori, I.B. McInnes, G. Valesini, and C. Pitzalis. 2004. Increased circulating levels and salivary gland expression of interleukin-18 in patients with Sjogren's syndrome: relationship with autoantibody production and lymphoid organization of the periductal inflammatory infiltrate. *Arthritis Res. Ther.* 6:447–456.
37. Muhl, H., and J. Pfeilschifer. 2004. Interleukin-18 bioactivity: a novel target for immunopharmacological anti-inflammatory intervention. *Eur. J. Pharmacol.* 500:63–71.
38. Hurgin, V., D. Novick, and M. Rubinstein. 2002. The promoter of IL-18 binding protein: activation by an IFN-γ-induced complex of IFN regulatory factor 1 and CCAAT/enhancer binding protein-β. *Proc. Natl. Acad. Sci. USA.* 99:16957–16962.
39. Paulukat, J., M. Bosmann, M. Nold, S. Garkisch, H. Kämpfer, S. Frank, J. Raedle, S. Zeuzem, J. Pfeilschifter, and H. Mühl. 2001. Expression and release of IL-18 binding protein in response to IFN-γ. *J. Immunol.* 167:7038–7043.
40. Baccala, R., and A.N. Theofilopoulos. 2005. The new paradigm of T-cell homeostatic proliferation-induced autoimmunity. *Trends Immunol.* 26:5–8.
41. King, C., A. Ilic, K. Koelsch, and N. Sarvetnick. 2004. Homeostatic expansion of T cells during immune insufficiency generates autoimmunity. *Cell.* 117:266–277.
42. Carrasco-Marin, E., J. Shimizu, O. Kanagawa, and E.R. Unanue. 1996. The class II MHC I-Ag7 molecules from non-obese diabetic mice are poor peptide binders. *J. Immunol.* 156:450–458.
43. Rasooly, L., C.L. Burek, and N.R. Rose. 1996. Iodine-induced autoimmune thyroiditis in NOD-H-2h4 mice. *Clin. Immunol. Immunopathol.* 81:287–292.
44. Qian, Y.W., Y.C. Wang, R.E. Hollingsworth Jr., D. Jones, N. Ling, and E.Y. Lee. 1993. A retinoblastoma-binding protein related to a negative regulator of Ras in yeast. *Nature.* 364:648–652.
45. Nicolas, E., S. Ait-Si-Ali, and D. Trouche. 2001. The histone deacetylase HDAC3 targets RbAp48 to the retinoblastoma protein. *Nucleic Acids Res.* 29:3131–3136.
46. Lai, A., J.M. Lee, W.M. Yang, J.A. DeCaprio, W.G. Kaelin Jr., E. Seto, and P.E. Branton. 1999. RBP1 recruits both histone deacetylase-dependent and -independent repression activities to retinoblastoma family proteins. *Mol. Cell. Biol.* 19:6632–6641.
47. Nicolas, E., V. Morales, L. Magnaghi-Jaulin, A. Harel-Bellan, H. Richard-Foy, and D. Trouche. 2000. RbAp48 belongs to the histone deacetylase complex that associates with the retinoblastoma protein. *J. Biol. Chem.* 275:9797–9804.
48. Szende, B., I. Romics, and L. Vass. 1993. Apoptosis in prostate cancer after hormonal treatment. *Lancet.* 342:1422.
49. Spyridopoulos, I., A. Sullivan, M. Kearney, J. Isner, and D. Losordo. 1997. Estrogen-receptor-mediated inhibition of human endothelial cell apoptosis. Estradiol as a survival factor. *Circulation.* 95:1505–1514.
50. Pelzer, T., M. Schumann, M. Neumann, T. deJager, M. Stimpel, E. Serfling, and L. Neyses. 2000. 17β-estradiol prevents programmed cell death in cardiac myocytes. *Biochem. Biophys. Res. Commun.* 268:192–200.
51. Pike, C.J. 1999. Estrogen modulates neuronal Bcl-xL expression and beta-amyloid-induced apoptosis: relevance to Alzheimer's disease. *J. Neurochem.* 72:1552–1563.
52. Bouker, K.B., T.C. Skaar, D.R. Fernandez, K.A. O'Brien, R.B. Riggins, D. Cao, and R. Clarke. 2004. Interferon regulatory factor-1 mediates the proapoptotic but not cell cycle arrest effects of the steroidal antiestrogen ICI 182,780 (faslodex, fulvestrant). *Cancer Res.* 64:4030–4039.
53. Davidson, A., and B. Diamond. 2001. Autoimmune diseases. *N. Engl. J. Med.* 345:340–350.
54. Marrack, P., J. Kappler, and B.L. Kotzin. 2001. Autoimmune disease: why and where it occurs. *Nat. Med.* 7:899–905.
55. Cenci, S., G. Toraldo, M.N. Weitzmann, C. Roggia, Y. Gao, and W.P. Qian. 2003. Estrogen deficiency induces bone loss by increasing T cell proliferation and lifespan through IFN-gamma-induced class II transactivator. *Proc. Natl. Acad. Sci. USA.* 100:10405–10410.
56. Hodgin, J.B., and N. Maeda. 2002. Minireview: estrogen and mouse models of atherosclerosis. *Endocrinology.* 143:4495–4501.
57. Mikkelsen, T.R., J. Brandt, H.J. Larsen, B.B. Larsen, K. Poulsen, J. Ingerslev, N. Din, and J.P. Hjorth. 1992. Tissue-specific expression in the salivary glands of transgenic mice. *Nucleic Acids Res.* 20:2249–2255.
58. White, S.C., and G.W. Casarett. 1974. Induction of experimental autoallergic sialadenitis. *J. Immunol.* 122:178–185.
59. Saegusa, K., N. Ishimaru, K. Yanagi, R. Arakaki, K. Ogawa, I. Saito, N. Katunuma, and Y. Hayashi. 2002. Cathepsin S-inhibitor prevents autoantigen presentation and autoimmunity. *J. Clin. Invest.* 110:361–369.

Development of Inflammatory Bowel Disease in Long-Evans Cinnamon Rats Based on $CD4^+CD25^+Foxp3^+$ Regulatory T Cell Dysfunction[1]

Naozumi Ishimaru,[2]* Akiko Yamada,* Masayuki Kohashi,* Rieko Arakaki,* Tetsuyuki Takahashi,† Keisuke Izumi,† and Yoshio Hayashi*

A mutant strain with defective thymic selection of the Long-Evans Cinnamon (LEC) rat was found to spontaneously develop inflammatory bowel disease (IBD)-like colitis. The secretion of Th1-type cytokines including IFN-γ and IL-2 from T cells of mesenteric lymph node cells (MLNs) and lamina propria mononuclear cells, but not spleen cells, in LEC rats was significantly increased more than that of the control Long-Evans Agouti rats through up-regulated expression of T-bet and phosphorylation of STAT-1 leading to NF-κB activation. In addition, the number of $CD4^+CD25^+Foxp3^+$ regulatory T (Treg) cells of the thymus, MLNs, and lamina propria mononuclear cells from LEC rats was significantly reduced, comparing with that of the control rats. Moreover, bone marrow cell transfer from LEC rats into irradiated control rats revealed significantly reduced $CD25^+Foxp3^+$ Treg cells in thymus, spleen, and MLNs compared with those from control rats. Indeed, adoptive transfer with T cells of MLNs, not spleen cells, from LEC rats into SCID mice resulted in the development of inflammatory lesions resembling the IBD-like lesions observed in LEC rats. These results indicate that the dysfunction of the regulatory system controlled by Treg cells may play a crucial role in the development of IBD-like lesions through up-regulated T-bet, STAT-1, and NF-κB activation of peripheral T cells in LEC rats. *The Journal of Immunology,* **2008, 180: 6997–7008.**

Inflammatory bowel disease (IBD)[3] in humans has two manifestations including Crohn's disease and ulcerative colitis (1–3). Although the precise mechanisms of the diseases are unknown, it has been reported that activation of the intestinal immune system in response to bacterial Ags with pathologic cytokine production of intestinal T cells through various transcription factors or signal molecules such as T-bet, GATA-3, and STATs plays a key role in the pathogenesis of IBD (4–7). The cytokine production by T cells is known to initiate and develop chronic intestinal inflammation (8–10). Crohn's disease is associated with Th1 cytokines such as IFN-γ and TNF-α (11, 12). Meanwhile, ulcerative colitis in human is associated with Th2 cytokine such as IL-5 (13). In addition, it is suggested that Th3 cytokine such as TGF-β has the immunosuppressive effect of IBD in human and animal models (14, 15). Furthermore, it is reported that nucleotide-binding oligomerization domain-containing proteins expressed in intestinal epithelial cells or APCs play a crucial role in the Th1 response in Crohn's disease (16–19). However, the pathogenesis based on cytokine balance of peripheral T cells for IBD is still unclear.

$CD4^+CD25^+$ regulatory T (Treg) cells have been widely studied in controlling inflammatory diseases including IBD (20–23). It is well known that the IBD model, by transfer of naive $CD45RB^{high}CD4^+$ T cells into T cell-deficient mice, can be controlled by coinjection of Treg cells to suppress $CD4^+$ effector T cell functions such as IFN-γ production (24). It has been reported that the cell number of Treg in the periphery from IBD patients was significantly reduced, or soluble IL-2Rα (CD25) of sera from IBD patients was increased (25, 26). However, it is obscure how natural Treg cells generated from thymus influence the pathogenesis of IBD.

Many animal models—such as C3H/HeJBir, IL-2-deficient, IL-2R-deficient, and IL-10-deficient mice, and HLA-B27/β2 transgenic rats—are known to be referred to as human IBD (27–31). It has been reported that the disease is induced by the hyperresponsiveness of T cells which is shifted to Th1 or Th2 cytokine production in each model (11–13). Cytokines produced by lamina propria (LP) $CD4^+$ T lymphocytes appear to initiate and perpetuate chronic intestinal inflammation. It is also reported that Th1 or Th2 cytokine production in IBD models can be modulated by the immunosuppressive cytokine such as TGF-β secreted by Th3 cells (22, 23). In addition, some transcription factors including T-bet and GATA-3 or signal molecules such as STATs are well known to regulate immunopathogenic or immunosuppressive cytokine production for controlling IBD (7).

The Long-Evans Cinnamon (LEC) rat was first described to be a naturally occurring mutant with a specific defect in thymocyte development, which has contained T cell differentiation arrest

*Department of Oral Molecular Pathology, Institute of Health Biosciences, University of Tokushima Graduate School, Kuramotocho, Tokushima, Japan; and †Department of Molecular and Environmental Pathology, Institute of Health Biosciences, University of Tokushima Graduate School, Kuramotocho, Tokushima, Japan

Received for publication August 24, 2007. Accepted for publication March 13, 2008.

The costs of publication of this article were defrayed in part by the payment of page charges. This article must therefore be hereby marked *advertisement* in accordance with 18 U.S.C. Section 1734 solely to indicate this fact.

[1] This work was supported in part by Grants-in-Aid for Scientific Research (17109016 and 17689049) from the Ministry of Education, Culture, Sports, Science, and Technology of Japan.

[2] Address correspondence and reprint requests to Dr. Naozumi Ishimaru, Department of Oral Molecular Pathology, Institute of Health Biosciences, University of Tokushima Graduate School, 3-18-15 Kuramotocho, Tokushima 770-8504, Japan. E-mail address: ishimaru@dent.tokushima-u.ac.jp

[3] Abbreviations used in this paper: IBD, inflammatory bowel disease; Treg, regulatory T; DP, double positive; SP, single positive; MLN, mesenteric lymph node cell; LP, lamina propria; BM, bone marrow; PAS, periodic acid Schiff; DAPI, 4′,6-diamidino-2-phenylindole; HPRT, hypoxanthine phosphoribosyltransferase; LPMC, LP mononuclear cell.

 0022-1767/08/$2.00

from $CD4^+CD8^+$ double-positive (DP) to $CD4^+CD8^-$ single-positive (SP) but not to $CD4^-CD8^+$ SP thymocytes (32). In addition, peripheral $CD4^+$ T cells of LEC rats were shown not to function as Th cells in Ab production against T cell-dependent Ag and IL-2 production by polyclonal stimulation (32, 33). However, it remains unclear whether the T cell dysfunction of LEC rats might have an influence on any disease associated with the immune disorder. In the present study, we found for the first time that IBD-like lesions developed spontaneously in LEC rats. Thus, the pathogenesis and molecular mechanisms of inflammatory bowel lesions in LEC rats as a human IBD model were analyzed.

Materials and Methods

Animals

LEC rats and LEA rats as controls were maintained in our laboratory under specific pathogen-free conditions. SCID mice (C.B-17/*Icr-scid/scid Jcl*) were purchased from CLEA Japan for use as recipients of adoptive transfer. The experiments were approved by an animal ethics board of Tokushima University.

Pathological analysis

All organs of rats and recipient mice were removed and fixed in 10% phosphate-buffered formaldehyde (pH 7.2), embedded in paraffin, and prepared for histological estimation. The sections were stained with H&E. The disease incidence was evaluated by three independent, well-trained pathologists in a blinded manner.

Flow cytometric analysis

Surface markers on lymphocytes from thymus, spleen, mesenteric lymph node cells (MLNs), and LP were analyzed by using an EPICS flow cytometer (Beckman Coulter) using FITC-, PE-Cy5-, or PE-conjugated anti-CD4, -CD8, -CD44, -CD62L, and -CD25 mAbs (BD Biosciences). To evaluate intracellular Foxp3 expression, lymphocytes were stained with anti-CD4 and -CD25 mAb, fixed and permeabilized with the buffers of a Foxp3 detection kit (BD Biosciences). After staining with anti-Foxp3 mAb, the lymphocytes were analyzed by flow cytometry.

Proliferation assay

T cells (>90%) were enriched from single-cell suspensions of spleen and lymph node cells from LEC, control rats, and SCID mice with nylon wool (Wako Pure Chemical), and cultured in 96-well flat-bottom microtiter plates (5×10^4 cells/well) in RPMI 1640 containing 10% FCS, penicillin/streptomycin, and 2-ME. Cells were stimulated with plate-coated anti-CD3 (BD Biosciences) and anti-CD28 mAb (BD Biosciences). [^{3}H]Thymidine incorporation during the last 12 h of the culture for 72 h was evaluated using an automated β liquid scintillation counter. In addition, to detect cell proliferation of the T cell subset, after CFSE (Molecular Probes)-labeled T cells were cultured for 48 h, the T cells were stained with anti-CD4 and -CD8 mAb. Cell divisions of $CD4^+$- or $CD8^+$-gated T cells were analyzed by flow cytometry. For T cell suppression assay, $CD25^-CD4^+$ or $CD25^+CD4^+$ T cells of MLN from control or LEC rats were enriched using biotin-conjugated anti-CD25 mAb, anti-CD4 mAb (BD Biosciences), magnetic beads, and the CELLection Biotin Binder kit (Dynal Biotech). A total of 5×10^4 $CD25^-CD4^+$ T cells from control rats were stimulated with plate-coated anti-CD3 mAb (0.5 μg/ml) for 72 h together with 0, 0.625, 1.25, and 2.5×10^4 $CD25^+CD4^+$ T cells from control or LEC rats. [^{3}H]Thymidine incorporation during the last 12 h of the culture was evaluated using an automated β liquid scintillation counter.

ELISA

Cytokine production was tested by a solid-phase sandwich ELISA using a rat IL-2, IL-4, IFN-γ, and IL-10 kit (BioSource International). In brief, culture supernatants from T cells from lymph nodes or spleen stimulated with anti-CD3 and -CD28 mAbs for 24 h and were added to microtiter plates precoated with an each Ab specific for rat L-2, IL-4, IFN-γ, and IL-10. The biotinylated Ab was added and the plate was incubated for 2 h at room temperature. After washing, streptavidin-HRP solution was added to each well and the plate was incubated for 30 min at room temperature. Finally, stabilized chromogen substrate was added to each well, and the absorbance of each well was read at 450 nm using an automatic microplate reader (Bio-Rad). The concentrations of cytokines were obtained according to the standard curves.

Western blot analysis

Isolated T or $CD4^+$ T cells from spleen and lymph nodes using nylon wool (Wako Pure Chemical) or PE-conjugated CD4 mAb with a magnetic PE selection kit (StemCell Technologies) were stimulated with anti-CD3/-CD28 mAbs for 12~24 h, washed, pelleted, and incubated in 20 mM/L Tris-HCl (pH 8.0), 20 mM/L NaCl, 0.5% Triton X-100, 5 mM/L EDTA, and 3 mM/L $MgCl_2$ lysis buffer including protease inhibitor mixture (Sigma-Aldrich). After centrifugation for 20 min at 12,000 rpm, supernatant was extracted and used as whole cell lysates. The nuclear extracts were purified using a Nuclear/Cytosol Fraction kit (BioVision). A total of 5~20 μg of each sample per well was applied for each well and electrophoresed in 10% SDS-polyacrylamide gel. Then, the protein was electrophoretically transferred to polyvinylidene difluoride membrane. The membrane was incubated with anti-T-bet, -GATA-3, -STAT-1, -phospho-STAT1, -GAPDH, -histone (Santa Cruz Biotechnology), and -Foxp3 (eBioscience) as the primary Abs. HRP-conjugated rabbit or mouse IgG was used as the second Ab. Protein binding was visualized with ECL Western blotting reagent (Amersham Biosciences). To quantify the protein expression, the chemiluminescence image was analyzed by ChemiDoc XRS (Bio-Rad).

Cell transfer

Bone marrow cells (5×10^6) from LEC and control rats were transferred i.v. into irradiated (4 Gy) control rats. Four weeks after the transfer, the host rats were analyzed. As for adoptive transfer to induce IBD-like lesions, purified T cells (5×10^6) from MLNs or spleen cells of LEC and control rats with nylon wool (Wako Pure Chemical) as donors were used and transferred i.p. into SCID mice. Six weeks after the transfer, the recipient SCID mice were sacrificed and all organs were histologically analyzed. In addition, MLN cells of SCID mice were cultured, and cytokine productions of the supernatants of the cells were analyzed by ELISA.

Injection of neutralizing Abs

A total of 50 μg of anti-rat IFN-γ mAb (PBL Biomedical Laboratories), anti-rat IL-4 mAb (R&D Systems), anti-rat CD8 mAb (BD Biosciences), and isotype control Ab were injected i.v. twice a week into LEC rats from 8 to 10 wk of age. Colon sections were stained with H&E and periodic acid Schiff (PAS), and the pathology was scored blindly using a semiquantitative scale of 0–5 as described previously (34). In summary, grade 0 was assigned when no changes were observed; grade 1, minimal inflammatory infiltrates present in the LP with or without mild mucosal hyperplasia; grade 2, mild inflammation in the LP with occasional extension into the submucosa, focal erosions, minimal to mild mucosal hyperplasia and minimal to moderate micin depletion; grade 3, mild to moderate inflammation in the LP and submucosa occasionally transmural with ulceration and moderate mucosal hyperplasia and mucin depletion; grade 4, marked inflammatory infiltrates commonly transmural with ulceration, marked mucosal hyperplasia and mucin depletion, and multifocal crypt necrosis; grade 5, marked transmural inflammation with ulceration, widespread crypt necrosis, and loss of intestinal glands.

Immunofluorescence staining and confocal microscopic analysis

Frozen sections of colon from LEC and control rats were fixed with 3% paraformaldehyde in PBS, and preblocked with 1% BSA-2.5% FCS in PBS for 1 h. Sections were stained with 1 μg/ml of primary Abs against CD4, CD8, CD45R, CD11b/c (BD Biosciences), T-bet, NF-κB, GATA-3, and phospho-STAT1 (Santa Cruz Biotechnology) for 1 h. After three washes in PBS, the sections were stained with Alexa Fluor 488 donkey anti-mouse IgG (H+L) or goat anti-rabbit IgG (H+L) (Molecular Probe) as the second Abs for 30 min and washed with PBS. The section stained with intracellular proteins were stained with PE-labeled anti-CD4 mAb. The nuclei was stained with 4',6-diamidino-2-phenylindole (DAPI). The sections were visualized with a laser scanning confocal microscope (Carl Zeiss). A 63 × 1.4 oil differential interference contrast objective lens was used. Quick Operation Version 3.2 (Carl Zeiss) for imaging acquisition and Adobe Photoshop CS2 (Adobe Systems) for image processing were used.

Real-time quantitative RT-PCR

Total RNA was extracted from purified lymphocytes of the thymus, spleen, and MLNs in LEC and control rats using Isogen (Wako Pure Chemical), and was reverse transcribed as described (35). Transcript levels of Foxp3 and hypoxanthine phosphoribosyltransferase (HPRT) were performed using PTC-200 DNA Engine Cycler (MJ Research) with SYBR Premix Ex Tag (Takara). The primer sequences were as follows: Foxp3: forward, 5'-CCCAGGAAAGACAGCAACCTT-3' and reverse, 5'-CTGCT TGGCAGTGCTTGAGAA-3'; and HPRT: forward, 5'-TGTTGGATACAG